ELSEVIER

On Reynolds-stress expressions and near-wall scaling parameters for predicting wall and homogeneous turbulent shear flows

K. Abe and T. Kondoh
Toyota Central Research and Development Laboratories, Inc., Aichi, Japan

Y. Nagano
Department of Mechanical Engineering, Nagoya Institute of Technology, Nagoya, Japan

In this paper, a new type of two-equation turbulence model that incorporates some essential characteristics of second-order closure models is proposed. The present model belongs to a nonlinear k-ε model taking into account low-Reynolds-number effects originating from the physical requirements, and is applicable to complex turbulent flows with separation and reattachment. The model successfully predicts both wall-turbulent and homogeneous shear flows, the latter of which has been very difficult to simulate with existing two-equation turbulence models. Channel flows with injection and suction at wall surfaces and separated and reattaching flows downstream of a backward-facing step are also calculated. Comparisons of the computational results with the measurements and the direct numerical simulation data indicate that the present model is effective in calculating complex turbulent flows of technological interest. Furthermore, the parameters for scaling the near-wall region in the low-Reynolds-number model functions are re-evaluated, yielding some insights into the near-wall scaling parameters for application to complex turbulent flows.

Keywords: two-equation model; second-moment closure; Kolmogorov scale; low-Reynolds-number model; wall turbulent flow; homogeneous shear flow

Introduction

The low-Reynolds-number (LRN) k-ε model is a powerful tool for predicting various turbulent flows encountered in almost every field of technology. Since the 1980–1981 Stanford Conference (Kline et al. 1981), a great deal of effort has gone into the development and improvement of the model in this category. In particular, the near-wall limiting behavior of turbulence was discussed in detail, and several models representing the correct behavior were proposed, among which the earliest were those developed by Myong and Kasagi (1990) and by Nagano and Tagawa (1990) (hereafter referred to as the NT model). Recently, based on these models, various types of k-ε models have been constructed. For example, Abe et al. (1994) proposed an improved version of the NT model. The most essential improvement made in this model is that the Kolmogorov velocity scale $u_\varepsilon \equiv (\nu\varepsilon)^{1/4}$ is introduced instead of the friction velocity u_τ to account for the near-wall and LRN effects. The velocity scale u_ε vanishes at neither the separating nor the reattaching points in contrast to the friction velocity u_τ, so that this model is applicable to separated and reattaching flows (Abe et al. 1994). The model by Nagano and Shimada (1995) reproduces the correct budgets not only of turbulent energy but also of its dissipation rate, in agreement with the direct numerical simulation (DNS) database (Kim et al. 1990).

Although these recent k-ε models are very useful, major problems remain concerning the eddy-viscosity approximation, $-\overline{u_i u_j} = \nu_t(\partial \overline{U}_i/\partial x_j + \partial \overline{U}_j/\partial x_i) - 2k\delta_{ij}/3$ with $\nu_t = C_\mu k^2/\varepsilon$. The most crucial problem is that the standard type of k-ε models cannot predict wall-turbulent and homogeneous shear flows without changing model constants; e.g., $C_\mu = 0.09$ (Suzuki et al. 1993; Tzuoo et al. 1986; Yoshizawa 1993; Yoshizawa and Nisizima 1993; Shih et al. 1994; Yakhot et al. 1992). Many remedies have been tried to overcome this difficulty, notably a zonal approach (Tzuoo et al. 1986), a nonequilibrium eddy-viscosity model (Yoshizawa 1993; Yoshizawa and Nisizima 1993),

Address reprint requests to Dr. Ken-ichi Abe, Applied Mathematics and Physics Lab., Toyota Central Research and Development Laboratories, Inc., Nagakute-cho, Aichi-gun, Aichi-ken 480-11, Japan.

Received 20 May 1996; accepted 30 August 1996

Int. J. Heat and Fluid Flow 18: 266–282, 1997

655 Avenue of the Americas, New York, NY 10010

0142-727X/97/$17.00
PII S0142-727X(97)00008-8

and modifications of the model constants using the mean-velocity gradient (Shih et al. 1994; Yakhot et al. 1992).

On the other hand, to advance a turbulence model, it is quite useful to refer to the models constructed on the basis of higher-order approximation. Pope (1975) showed the explicit expression of the Reynolds stress, $\overline{u_i u_j}$, for a two-dimensional (2-D) algebraic stress model (ASM). Taulbee (1992) developed a new type of explicit ASM expression (EASM) and a nonlinear k-ε formulation on the basis of discussions made by Pope and applied them to a homogeneous shear flow, a plain strain flow, and a stagnation flow. However, this model has not been applied to wall-turbulent flows. Thus, the development of more sophisticated two-equation models applicable to both wall and homogeneous turbulent shear flows is awaited. Gatski and Speziale (1993) recently extended Pope's idea to a three-dimensional (3-D) formula and discussed the relation between the EASM expression and the nonlinear k-ε formulation proposed by Speziale (1987). The understanding obtained from this discussion is worth noting for the development of the coming generation of two-equation models.

In this study, we propose a new type of k-ε model that incorporates some essential characteristics of Reynolds stress and algebraic stress models. The present model belongs to a nonlinear k-ε model and is suitably reduced to an LRN k-ε model by employing the Kolmogorov velocity scale u_ε to reproduce near-wall limiting behavior and to be applicable to complex turbulent flows with separation and reattachment (Abe et al. 1994). To verify the model performance, the proposed model is tested by application to some fundamental turbulent flows; i.e., a fully developed channel flow and a homogeneous shear flow. It is also applied to complex turbulent flows; i.e., channel flows with injection and suction at wall surfaces, and separated and reattaching flows downstream of a backward-facing step.

Furthermore, the LRN parameters in the model functions are re-examined by comparing the computational results of the present model with those by representative LRN k-ε models. Recently, many types of LRN k-ε models have been proposed in which various types of LRN parameters were adopted. However, there has been little discussion of whether or not the asymptotic scale used in the model is reasonable in scaling the near-wall

Notation

b_{ij}	anisotropy tensor, $\overline{u_i u_j}/2k - \delta_{ij}/3$
C_f	skin friction coefficient
$C_{\varepsilon 1}, C_{\varepsilon 2}$	constants in transport equation for ε
$C_\mu, C_D, C_\eta, C_s, C_\varepsilon$	model constants
D/Dt	substantial derivative, $\partial/\partial t + \overline{U}_j \partial/\partial x_j$
ER	expansion ratio of widths of downstream and upstream channels
$f_{,i}$	partial derivative of variable f with respect to coordinate x_i
$f_\mu, f_\varepsilon, f_B, f_{t1}, f_{t2}$	model functions
H	height of backward-facing step; shape factor
h	wind-tunnel exit width
k	turbulent kinetic energy, $\overline{u_i u_i}/2$
L	length of one period of injection and suction, $4\pi\delta$
l_K	Kolmogorov length scale, $(\nu^3/\varepsilon)^{1/4}$
l_T	Taylor microscale, $(\nu k/\varepsilon)^{1/2}$
N_ξ, N_η	number of grid points in ξ- and η-directions
n	distance between a point and the nearest point on the whole wall surface in flow field
n^*	nondimensional distance, $u_\varepsilon n/\nu$
$\bar{P}, p$	mean static pressure and pressure fluctuation
P_k	production term of k, $-\overline{u_i u_j}\overline{U}_{i,j}$
P_{ij}	production term of Reynolds stress, $-\overline{u_i u_k}\overline{U}_{j,k} - \overline{u_j u_k}\overline{U}_{i,k}$
R_t	turbulent Reynolds number, $k^2/\nu\varepsilon$
Re_H	Reynolds number based on step height, $\overline{U}_0 H/\nu$
Re_x	Reynolds number based on distance from leading edge, $\overline{U}_0 x/\nu$
Re_τ	Reynolds number based on friction velocity, $u_\tau\delta/\nu$ or $u_\tau^{**}\delta/\nu$
Re_θ	Reynolds number based on momentum thickness, $\overline{U}_0\theta/\nu$
S_{ij}	strain-rate tensor, $(\overline{U}_{i,j} + \overline{U}_{j,i})/2$
t	time
$\overline{U}_0$	reference velocity
$\overline{U}, \overline{V}$	mean velocity in x- and y-directions
$\overline{U}_i, u_i$	mean velocity and turbulent fluctuation in i-direction
$\overline{U}^+$	nondimensional mean velocity, $\overline{U}/u_\tau$
u, v	turbulent fluctuation in x- and y-directions
u_ε	Kolmogorov velocity scale, $(\nu\varepsilon)^{1/4}$
u_τ	friction velocity
u_τ^{**}	averaged friction velocity on both side walls
x, y	Cartesian coordinates in longitudinal (streamwise) and lateral directions
X_R	flow reattachment length
x_i	Cartesian coordinate in i-direction
y^+	nondimensional distance from wall surface, $u_\tau y/\nu$
$(\bar{\ })$	ensemble-averaged value
Greek	
δ	half width of channel
δ_{ij}	Kronecker delta
δ_0	99% boundary-layer thickness
ε	dissipation rate of turbulent kinetic energy, $\nu\overline{u_{i,j}u_{i,j}}$
ε_{ij}	dissipation-rate tensor, $2\nu\overline{u_{i,k}u_{j,k}}$
η	generalized coordinate in lower- to upper-wall direction
θ	momentum thickness at step location
ν, ν_t	kinematic and eddy-viscosities
ξ	generalized coordinate from inlet to outlet
ρ	density
τ	characteristic time scale for turbulence
τ_K	Kolmogorov time scale, $(\nu/\varepsilon)^{1/2}$
Φ_{ij}	pressure-strain correlation, $\overline{(p/\rho)(u_{i,j} + u_{j,i})}$
Ω_{ij}	vorticity tensor, $(\overline{U}_{i,j} - \overline{U}_{j,i})/2$

turbulence from the physical viewpoints. Therefore, we investigate here representative near-wall scaling parameters in detail, resulting in several insights into what factors determine the LRN parameters used in the model functions.

Turbulence modeling

Governing equations

The governing equations for an incompressible turbulent velocity field with a k-ε model can be expressed as follows (i.e., the equation of continuity, the ensemble-averaged Navier–Stokes equation, and the transport equations of the turbulent energy and its dissipation rate):

$$\frac{\partial \bar{U}_i}{\partial x_i} = 0 \tag{1}$$

$$\frac{\mathrm{D}\bar{U}_i}{\mathrm{D}t} = -\frac{1}{\rho}\frac{\partial \bar{P}}{\partial x_i} + \frac{\partial}{\partial x_j}\left[\nu\left(\frac{\partial \bar{U}_i}{\partial x_j} + \frac{\partial \bar{U}_j}{\partial x_i}\right) - \overline{u_i u_j}\right] \tag{2}$$

$$\frac{\mathrm{D}k}{\mathrm{D}t} = \frac{\partial}{\partial x_j}\left[\nu\frac{\partial k}{\partial x_j} - \overline{\left(k' + \frac{p}{\rho}\right)u_j}\right] - \overline{u_i u_j}\frac{\partial \bar{U}_i}{\partial x_j} - \varepsilon \tag{3}$$

$$\frac{\mathrm{D}\varepsilon}{\mathrm{D}t} = \frac{\partial}{\partial x_j}\left(\nu\frac{\partial \varepsilon}{\partial x_j} - \overline{\varepsilon' u_j} - \frac{2\nu}{\rho}\frac{\partial p}{\partial x_i}\frac{\partial u_j}{\partial x_i}\right) - C_{\varepsilon 1}\frac{\varepsilon}{k}\overline{u_i u_j}\frac{\partial \bar{U}_i}{\partial x_j} - C_{\varepsilon 2} f_\varepsilon \frac{\varepsilon^2}{k} \tag{4}$$

where $k' = u_i u_i/2$, $\varepsilon' = \nu(\partial u_i/\partial x_k)(\partial u_i/\partial x_k)$ and $k = \overline{k'}$, $\varepsilon = \overline{\varepsilon'}$, respectively. In Equation 4, $C_{\varepsilon 1}$ and $C_{\varepsilon 2}$ are the model constants, and f_ε is the model function to satisfy the physical requirement in the near-wall region (Nagano and Tagawa 1990; Abe et al. 1994), as discussed in detail later.

Modeling Reynolds stress

In what follows, we construct a new type of expression of the Reynolds stress $\overline{u_i u_j}$ by introducing the EASM concept (Pope 1975; Taulbee 1992; Gatski and Speziale 1993) to the nonlinear k-ε formulation.

First, the transport equation for the anisotropy tensor $b_{ij}(=\overline{u_i u_j}/2k - \delta_{ij}/3)$ is expressed as follows (neglecting the diffusive effect):

$$\frac{\mathrm{D}b_{ij}}{\mathrm{D}t} = \frac{1}{2k}\left[\left(P_{ij} - \frac{2}{3}P_k\delta_{ij}\right) + \Phi_{ij} - \left(\varepsilon_{ij} - \frac{2}{3}\varepsilon\delta_{ij}\right)\right] - \frac{\varepsilon}{k}\left(\frac{P_k}{\varepsilon} - 1\right)b_{ij} \tag{5}$$

where P_{ij} and P_k respectively denote the production terms of Reynolds stress and turbulent energy; i.e., $P_{ij} = -\overline{u_i u_k}\bar{U}_{j,k} - \overline{u_j u_k}\bar{U}_{i,k}$ and $P_k = P_{ii}/2 = -\overline{u_i u_k}\bar{U}_{i,k}$. Here, $\bar{U}_{i,j}$ is the partial derivative of the mean velocity $\bar{U}_i$ with respect to the coordinate x_j (e.g., $\bar{U}_{1,2} = \partial\bar{U}_1/\partial x_2 = \partial\bar{U}/\partial y$, etc.). In Equation 5, $\Phi_{ij} = \overline{(p/\rho)(u_{i,j} + u_{j,i})}$ represents the pressure-strain correlation, and $\varepsilon_{ij} = 2\nu\overline{u_{i,k}u_{j,k}}$ is the dissipation-rate tensor. For these quantities, we introduce the following most general expression, which is tensorially linear in the anisotropy tensor b_{ij}.

$$\Phi_{ij} - \left(\varepsilon_{ij} - \frac{2}{3}\varepsilon\delta_{ij}\right) = -C_1\varepsilon b_{ij} + C_2 k S_{ij} + C_3 k\left(S_{ik}b_{kj} + b_{ik}S_{kj} - \frac{2}{3}b_{mn}S_{mn}\delta_{ij}\right) + C_4 k(\Omega_{ik}b_{kj} - b_{ik}\Omega_{kj}) \tag{6}$$

where C_1, C_2, C_3, and C_4 are the model constants, and $S_{ij}[=(\bar{U}_{i,j} + \bar{U}_{j,i})/2]$, and $\Omega_{ij}[=(\bar{U}_{i,j} - \bar{U}_{j,i})/2]$ are the strain-rate and

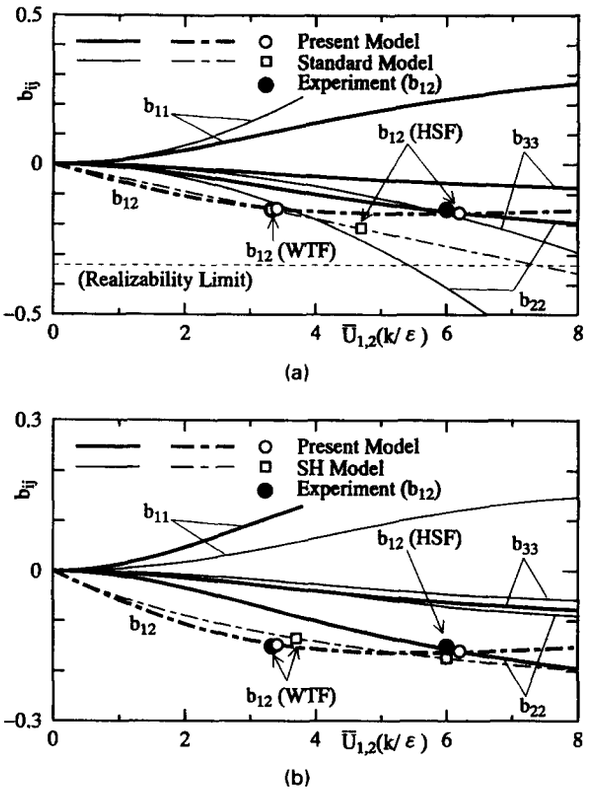

Figure 1 Relation between anisotropy tensors and shear parameter (WTF; wall-turbulent flow, HSF; homogeneous shear flow): (a) comparison with Standard nonlinear model; (b) comparison with Shih et al. (SH) model (1994)

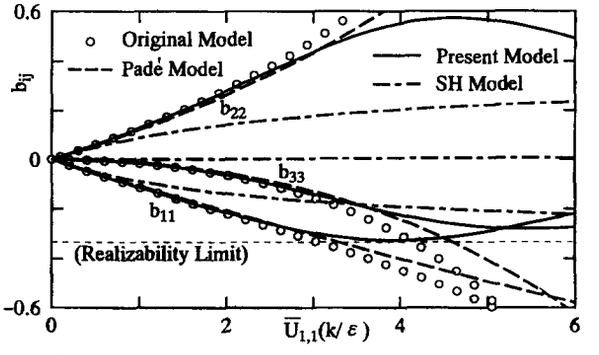

Figure 2 Anisotropy tensors versus normal strain rate

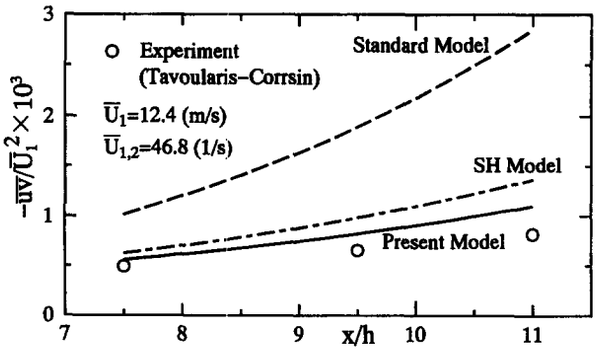

Figure 3 Reynolds shear-stress predictions in homogeneous shear flow

the vorticity tensors, respectively. In local equilibrium state, the following relation holds.

$$\frac{Db_{ij}}{Dt}=0 \tag{7}$$

Substituting Equation 6 for Equation 5 with the above condition (Equation 7) yields the relation given by

$$\frac{\varepsilon}{k}\left[C_1+2\left(\frac{P_k}{\varepsilon}-1\right)\right]b_{ij}$$

$$=\left(C_2-\frac{4}{3}\right)S_{ij}+(C_3-2)\left(S_{ik}b_{kj}+b_{ik}S_{kj}-\frac{2}{3}b_{mn}S_{mn}\delta_{ij}\right)$$

$$+(C_4-2)(\Omega_{ik}b_{kj}-b_{ik}\Omega_{kj}) \tag{8}$$

where the following time-scale is adopted as the characteristic time scale of turbulence:

$$\frac{1}{\left\{C_1+2\left(\frac{P_k}{\varepsilon}-1\right)\right\}}\left(\frac{k}{\varepsilon}\right) \tag{9}$$

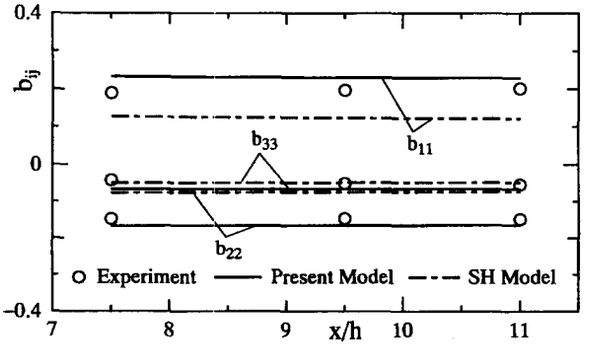

Figure 4 Anisotropy tensors for homogeneous shear flow

By introducing the nondimensional variables

$$b_{ij}^*=\left(\frac{2-C_3}{\frac{4}{3}-C_2}\right)b_{ij},\qquad S_{ij}^*=\frac{\left(\frac{k}{\varepsilon}\right)(2-C_3)}{\left[C_1+2\left(\frac{P_k}{\varepsilon}-1\right)\right]}S_{ij},$$

$$\Omega_{ij}^*=\frac{\left(\frac{k}{\varepsilon}\right)(2-C_4)}{\left[C_1+2\left(\frac{P_k}{\varepsilon}-1\right)\right]}\Omega_{ij} \tag{10}$$

and solving Equation 8 in the 2-D space, we can obtain the following formal expression for b_{ij}^* (hereafter referred to as the original model).

$$b_{ij}^*=\frac{3}{3+6\Omega^{*2}-2S^{*2}}\left[-S_{ij}^*-(S_{ik}^*\Omega_{kj}^*-\Omega_{ik}^*S_{kj}^*)\right.$$

$$\left.+2\left(S_{ik}^*S_{kj}^*-\frac{1}{3}S_{mn}^*S_{mn}^*\delta_{ij}\right)\right] \tag{11}$$

where $S^{*2}=S_{mn}^*S_{mn}^*$, and $\Omega^{*2}=\Omega_{mn}^*\Omega_{mn}^*$. The Reynolds-stress expression given by Equation 11 is expected to be applicable to many types of turbulent flows not unusually deviating from the equilibrium state, because it is directly obtained from the general expression for Φ_{ij} and ε_{ij} (Equation 6). This model, however, cannot express the correct turbulent phenomena in the near-wall region, where the viscous and turbulent diffusion becomes large,

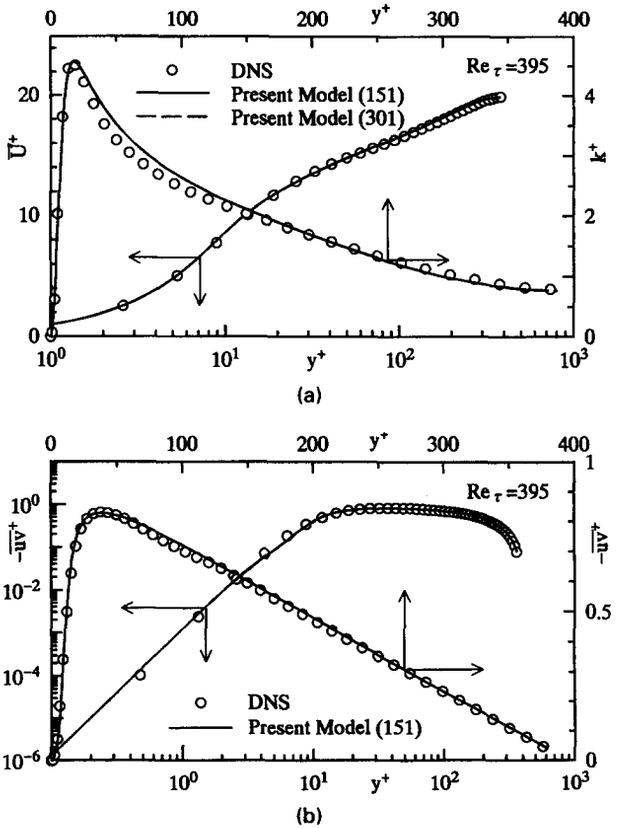

Figure 5 Computational results in channel flow: (a) mean velocity and turbulent energy; (b) Reynolds shear stress

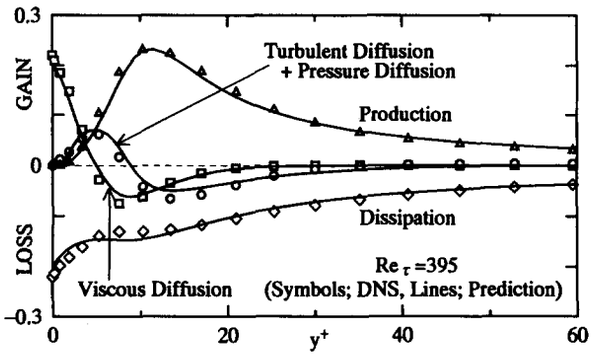

Figure 6 Budget of turbulent energy in channel flow

and a flow deviates greatly from local equilibrium state. In other words, the characteristic time-scale given by Equation 9 is not appropriate to representing the near-wall turbulence.

On the other hand, the nonlinear k-ε model of Speziale (1987) is expressed as follows.

$$\overline{u_i u_j} = \frac{2}{3}k\delta_{ij} - 2\nu_t S_{ij} - 4C_D\frac{\nu_t^2}{k}(S_{ik}\Omega_{kj} - \Omega_{ik}S_{kj})$$

$$+ 4C_D\frac{\nu_t^2}{k}\left(S_{ik}S_{kj} - \frac{1}{3}S_{mn}S_{mn}\delta_{ij}\right) \tag{12}$$

Note that the substantial derivative of the Oldroyd derivative in the original formulation (Speziale) is omitted here. The eddy-viscosity ν_t in Equation 12 is expressed as follows.

$$\nu_t = C_\mu f_\mu \frac{k^2}{\varepsilon} \tag{13}$$

where f_μ is the model function (not included in the original model, Speziale) to account for the near-wall and LRN effects originating from the physical requirements. By normalizing the anisotropy tensor b_{ij}, the strain-rate tensor S_{ij} and the vorticity tensor Ω_{ij} as

$$b_{ij}^* = C_D b_{ij}, \qquad S_{ij}^* = C_D\tau S_{ij}, \qquad \Omega_{ij}^* = 2C_D\tau\Omega_{ij} \tag{14}$$

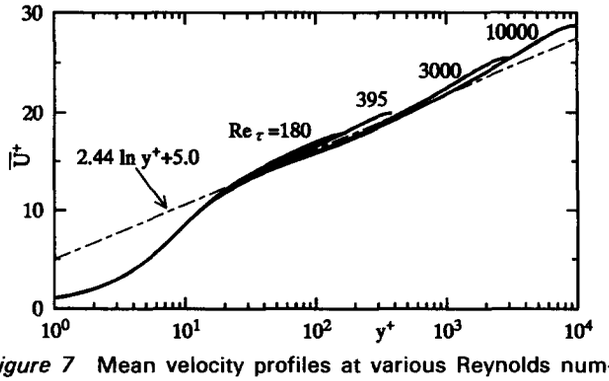

Figure 7 Mean velocity profiles at various Reynolds numbers

we can rewrite Equation 12 as follows (hereinafter referred to as the Standard model).

$$b_{ij}^* = -S_{ij}^* - (S_{ik}^*\Omega_{kj}^* - \Omega_{ik}^*S_{kj}^*)$$

$$+ 2\left(S_{ik}^*S_{kj}^* - \frac{1}{3}S_{mn}^*S_{mn}^*\delta_{ij}\right) \tag{15}$$

where C_D is the model constant and the following time-scale is employed as the characteristic time-scale of turbulence:

$$\tau = \frac{\nu_t}{k} = C_\mu f_\mu \frac{k}{\varepsilon} \tag{16}$$

The model above can express the anisotropy of the Reynolds stresses in wall shear flows. It cannot, however, give reasonable predictions for a homogeneous shear flow, because the Reynolds-stress expression is essentially the extension of the standard eddy-viscosity approximation.

Now, comparing Equations 11 and 15, we can easily understand that the contents of [ ] in Equation 11 completely coincide with Equation 15. This suggests that a more sophisticated k-ε model may be constructed by introducing the important aspects of the coefficient in front of [ ] in Equation 11. Thus, in this study, we propose the expression given by Equation 11 with the variables defined by Equation 14 as the basic representation for the Reynolds stress tensor, leading to an appropriate expression in both wall and homogeneous turbulent shear flows, and also in the regions both away from and close to the wall.

The Reynolds stress expression given by Equation 11 has, however, a significant problem; i.e., mathematical (phenomenological) inaccuracies may occur with the increase of S^{*2}, because the denominator of the coefficient can be zero or negative. As a solution, following Gatski and Speziale (1993), we can modify the coefficient using the Padé-type approximation (hereafter referred to as the Padé model) as follows.

$$\frac{3(1 + S^{*2})}{3 + S^{*2} + 6\Omega^{*2}S^{*2} + 6\Omega^{*2}} \tag{17}$$

The modification by Equation 17 is, however, still inadequate to promise to give non-negative turbulent intensities, although it guarantees a non-negative value of the coefficient. Therefore, in the present study, Equation 11 is re-examined and modified to assure non-negative turbulent intensities, as discussed below.

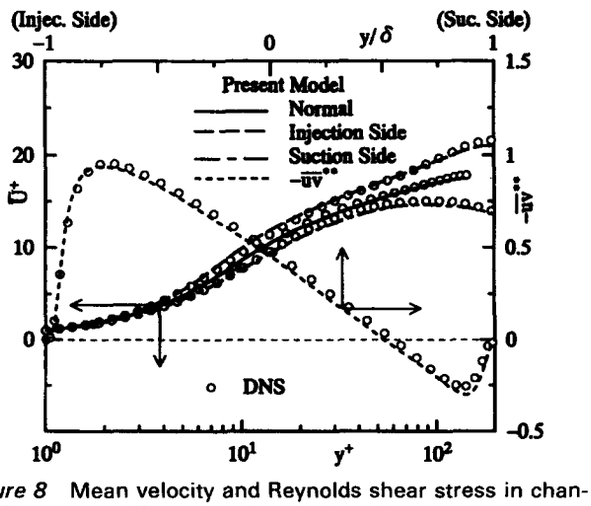

Figure 8 Mean velocity and Reynolds shear stress in channel flow with uniform injection and suction

First, we rewrite the coefficient of Equation 11 as follows:

$$\frac{3}{3+6\Omega^{*2}-2S^{*2}} = \frac{1}{1+\frac{22}{3}\left(\frac{\Omega^{*2}}{4}\right)+\frac{2}{3}\left(\frac{\Omega^{*2}}{4}-S^{*2}\right)} \tag{18}$$

The parameter $(\Omega^{*2}/4 - S^{*2})$ [i.e., $(1/2)(C_D\tau)^2(\Omega^2 - S^2)$, where $S^2 = 2S_{mn}S_{mn}$ and $\Omega^2 = 2\Omega_{mn}\Omega_{mn}$] in Equation 18 is one of the most important measures in turbulence, because it indicates how the flow field deviates from the condition of pure shear flow. As recognized from Equation 18, the foregoing mathematical inaccuracies do not occur in pure shear flows, where only S_{12}, $S_{21}(=S_{12})$, $\Omega_{12}(=S_{12})$ and $\Omega_{21}(=-S_{12})$ exist so that $(\Omega^{*2}/4 - S^{*2}) = 0$. On the contrary, improper behavior may result when the flow field greatly deviates from pure shear flow, because the normal strain rate is much larger than the shear strain rate; i.e., $S^{*2} \gg \Omega^{*2}/4$. On that basis, Equation 18 is modified as follows, in which a model function f_B is introduced to guarantee non-negative turbulent intensities under the condition of $S^{*2} \gg \Omega^{*2}/4$.

$$\frac{1}{1+\frac{22}{3}\left(\frac{\Omega^{*2}}{4}\right)+\frac{2}{3}\left(\frac{\Omega^{*2}}{4}-S^{*2}\right)f_B} \tag{19}$$

In Equation 19, it is desirable to model f_B so that its effect disappears in such pure shear flows as a fully developed channel flow and a homogeneous shear flow. Thus, we adopt the following simplest formulation, which satisfies these requirements.

$$f_B = 1 + C_\eta\left(\frac{\Omega^{*2}}{4} - S^{*2}\right) \tag{20}$$

where C_η is the model constant.

Thus, the final expression of the Reynolds stress in the present model is

$$b_{ij}^* = \frac{1}{1+\frac{22}{3}\left(\frac{\Omega^{*2}}{4}\right)+\frac{2}{3}\left(\frac{\Omega^{*2}}{4}-S^{*2}\right)f_B} \times\left[-S_{ij}^* - (S_{ik}^*\Omega_{kj}^* - \Omega_{ik}^*S_{kj}^*) + 2\left(S_{ik}^*S_{kj}^* - \frac{1}{3}S_{mn}^*S_{mn}^*\delta_{ij}\right)\right] \tag{21}$$

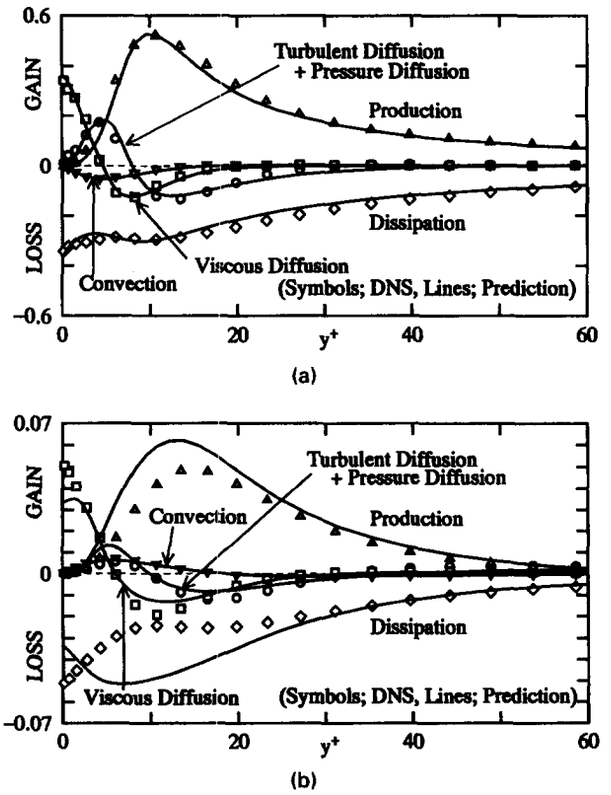

Figure 9 Budget of turbulent energy in channel flow with uniform injection and suction: (a) injection side; (b) suction side

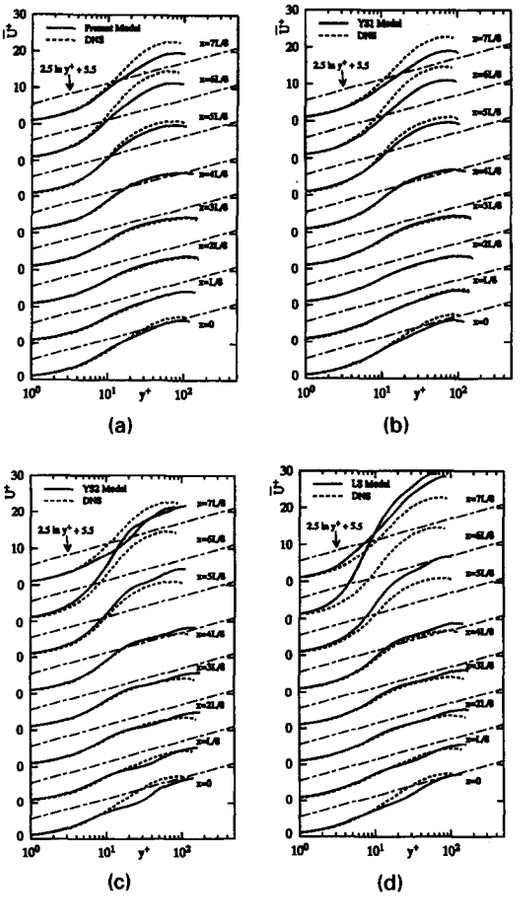

Figure 10 Mean-velocity profile in channel flow with periodic injection and suction at one side wall: (a) present model; (b) Yang–Shih (YS1) model; (c) Yang–Shih (YS2) model; (d) Launder–Sharma (LS) model

Note that the present model (Equation 21) can be rewritten as follows with the conventional form as in Equation 12.

$$\overline{u_i u_j} = \frac{2}{3}k\delta_{ij} + \frac{1}{1+\left(\frac{C_D\nu_t}{k}\right)^2\left[\frac{11}{3}\Omega^2+\frac{1}{3}(\Omega^2-S^2)f_B\right]} \times\left[-2\nu_t S_{ij} - 4C_D\frac{\nu_t^2}{k}(S_{ik}\Omega_{kj}-\Omega_{ik}S_{kj}) + 4C_D\frac{\nu_t^2}{k}\left(S_{ik}S_{kj}-\frac{1}{3}S_{mn}S_{mn}\delta_{ij}\right)\right] \quad (22)$$

Turbulent diffusion terms in Equations 3 and 4 are modeled using the generalized gradient diffusion hypothesis by Daly and Harlow (1970) as follows.

$$\overline{\left(k'+\frac{p}{\rho}\right)u_j} = -C_s f_{t1}\tau\overline{u_j u_l}\frac{\partial k}{\partial x_l} \quad (23)$$

$$\overline{\varepsilon' u_j} + \frac{2\nu}{\rho}\overline{\frac{\partial p}{\partial x_i}\frac{\partial u_j}{\partial x_i}} = -C_\varepsilon f_{t2}\tau\overline{u_j u_l}\frac{\partial \varepsilon}{\partial x_l} \quad (24)$$

where C_s and C_ε are the model constants, and f_{t1} and f_{t2} are the model functions activating in the vicinity of the wall, as described later.

The model constants are determined in a conventional manner. First, C_μ and C_D are set to 0.12 and 0.8, respectively, in order to represent properly equilibrium states in wall-turbulent ($\overline{U}_{1,2}k/\varepsilon \simeq 3.3$, $b_{12} \simeq -0.15$) and homogeneous shear ($\overline{U}_{1,2}k/\varepsilon \simeq 6$, $b_{12} \simeq -0.15$) flows (Tavoularis and Corrsin 1981) with the guarantee of non-negative turbulent intensities under the condition of $\overline{U}_{1,2}k/\varepsilon \gg 1$. In Equation 20, C_η is set to 5.0, so that non-negative turbulent intensities can be assured for any value of $\overline{U}_{1,1}k/\varepsilon$ ($= -\overline{U}_{2,2}k/\varepsilon$) in the 2-D flow field, and so that the influence of the model function f_B should be as small as possible. The model constant C_ε for the turbulent diffusion is set to 1.4 based on the relation for "constant stress layer" (Nagano and Tagawa 1990; Abe et al. 1994), and C_s is assigned the same value as C_ε; i.e., $C_s = 1.4$. To avoid confusion, some explanation of the model constants, C_ε and C_s, is appropriate. As described above, C_ε is set to 1.4 in the present model. The expression of ν_t, however, includes the model constant C_μ ($= 0.12$), so that the value corresponding to the conventional expression becomes $C_\varepsilon C_\mu \simeq 0.17$, which is essentially identical to that of 0.18 used in the Launder-Reece-Rodi (LRR) model (Launder et al. 1975). As for C_s, the value assessed in the same way is $C_s C_\mu \simeq 0.17$, which is slightly smaller than the value of 0.22 used in the LRR model. Recent studies (Myong and Kasagi 1990; Nagano and Tagawa), however, indicate that the turbulent diffusion in k in the region away from the wall is too diffusive when the conventional value is used. Thus, the present selection is reasonable and proper to reproduce the accurate profile of k given by the DNS (Kim et al. 1990) as shown later. In Equation 4, $C_{\varepsilon 1}$ and $C_{\varepsilon 2}$ are set to the generally accepted values; i.e., $C_{\varepsilon 1} = 1.45$ and $C_{\varepsilon 2} = 1.9$, respectively (Nagano and Tagawa).

Extension to a low-Reynolds-number model

The near-wall and LRN effects are modeled as follows. Concerning f_μ and f_ε, we basically follow the concept of Abe et al. (1994), taking account of some recent understandings suggested by Nagano and Shimada (1995). As a result, the present model

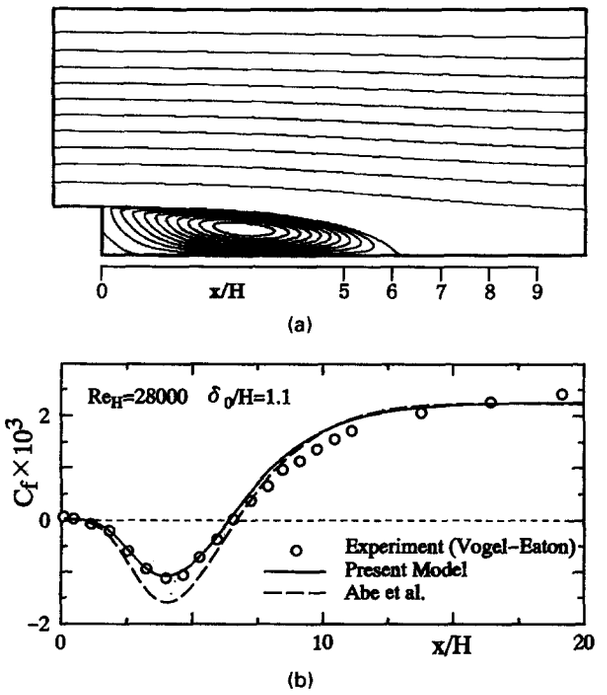

Figure 11 Computational results for Case 2: (a) Streamlines; (b) Skin friction coefficient

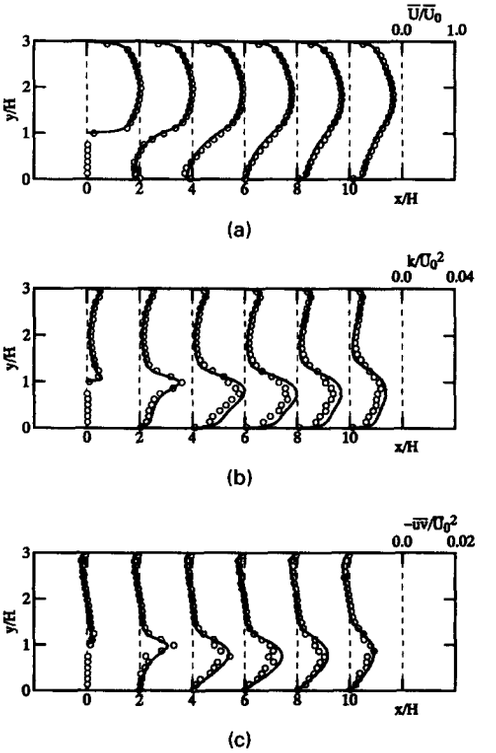

Figure 12 Comparison with experiment of Kasagi and Matsunaga (1995) (Case 3): O experiment; — prediction; (a) streamwise velocity; (b) turbulent energy; (c) Reynolds shear stress

functions become

$$f_\mu = \left\{1 + \frac{35}{R_t^{3/4}} \exp\left[-\left(\frac{R_t}{30}\right)^{3/4}\right]\right\}\left\{1 - \exp\left[-\left(\frac{n^*}{26}\right)^2\right]\right\} \quad (25)$$

$$f_\varepsilon = \left\{1 - 0.3\exp\left[-\left(\frac{R_t}{6.5}\right)^2\right]\right\}\left\{1 - \exp\left[-\left(\frac{n^*}{3.7}\right)^2\right]\right\} \quad (26)$$

where $n^*(=u_\varepsilon n/\nu)$ is the nondimensional wall distance, and $R_t(=k^2/\nu\varepsilon)$ is the turbulent Reynolds number. It is appropriate to discuss the argument regarding the use of the wall distance in the model functions. In this study, the wall distance at a point n is definitely determined by the definition as "the distance between that point and the nearest point on all the wall surfaces in a flow field." By following this definition, we can uniquely determine the wall distance n used in the model functions in any geometrical configuration and in any coordinate system. Even near the corner, it can be determined by considering the limit of a wall with a very small curvature. The distance between two points is not essentially harmful to the tensorial invariance, as is readily recognized by some expressions of the two-point correlation equations and a general solution of the pressure-strain correlation. Furthermore, we have confirmed that the calculations with the present model, in which the wall distance is uniquely determined by the above-mentioned definition, give the identical solution when the coordinate system is rotated some degrees; e.g., 45°, in backward-facing step flows. This is a logical consequence of the above discussions. Thus, it is concluded that the use of the wall distance does not violate the tensorial invariance, as long as the wall distance is determined uniquely in the problem; e.g., the nearest distance from all the wall surfaces as employed in the present study.

The most important feature of the present model functions is the introduction of the Kolmogorov velocity scale, $u_\varepsilon = (\nu\varepsilon)^{1/4}$, instead of the friction velocity u_τ, to account for the near-wall and LRN effects in both attached and detached flows (Abe et al. 1994). This model can reproduce the correct near-wall asymptotic relations of turbulence; i.e., $k \propto n^2$, $\varepsilon \propto n^0$, $\nu_t \propto n^3$ and $-\overline{uv} \propto n^3$ for $n \to 0$. It should be emphasized that the LRN model functions in the present model are not so-called "damping functions" but those introduced by the physical requirements in modeling the near-wall region. Considering the near-wall limiting behavior, the characteristic time scale $\tau(=\nu_t/k)$ in the present model is expressed as follows.

$$\tau = \frac{\nu_t}{k} = C_\mu f_\mu \frac{k}{\varepsilon} \to \frac{kn^{*2}}{\varepsilon R_t^{3/4}} \to \left(\frac{n^2}{l_K l_T}\right)\tau_K \quad (27)$$

where $l_K[=(\nu^3/\varepsilon)^{1/4}]$ is the Kolmogorov length scale, $l_T[=(\nu k/\varepsilon)^{1/2}]$ is the Taylor microscale and $\tau_K[=(\nu/\varepsilon)^{1/2}]$ is the Kolmogorov time-scale. In Equation 27, the Taylor microscale l_T is proportional to n in the near-wall region and n/l_T approaches the finite value of $2^{1/2}$. Therefore, in the proximity to the wall, the time-scale expressed by Equation 27 can be rewritten as follows.

$$\tau = \frac{\nu_t}{k} \to \left(\frac{n^2}{l_K l_T}\right)\tau_K \to \left(\frac{n}{l_K}\right)\tau_K \quad (28)$$

The time-scale $(n/l_K)\tau_K$ in Equation 28 is what is called the "quasi-Kolmogorov time scale," which is modified to satisfy the physical requirements for the exact wall-limiting behavior of turbulence. It is obvious that this time-scale is directly related to the Kolmogorov time scale and quite reasonable as the characteristic time scale representing the near-wall turbulent phenomena.

On the other hand, in the near-wall region, the viscous diffusion balances with the destruction term in the ε-equation as in the k-equation. Such a balance can be accomplished by switching the characteristic time-scale from the energy-containing time-scale k/ε to that which approaches a finite value in the vicinity of the wall. Taking into account the near-wall asymptotic relation, the characteristic time-scale of the destruction term in Equation 4 of the present model can be expressed as follows.

$$\frac{k}{\varepsilon f_\varepsilon} \to \frac{k}{\varepsilon n^{*2}} \to \left(\frac{l_T}{n}\right)^2 \tau_K \to \tau_K \quad (29)$$

Note that we use the relation of $(n/l_T \to 2^{1/2})$, as mentioned above. As can be readily seen, the characteristic time-scale of the present model given by Equation 29 is directly related to the Kolmogorov time scale τ_K. Hence, the characteristic time-scales in both Equations 28 and 29 are essentially identical and physically appropriate to account for the near-wall turbulence.

Concerning the turbulent diffusion, it is revealed by the recent DNS databases that the turbulent diffusion both in k and in ε becomes larger in the near-wall region (Nagano and Shimada 1995). Thus, we introduce the following model functions in

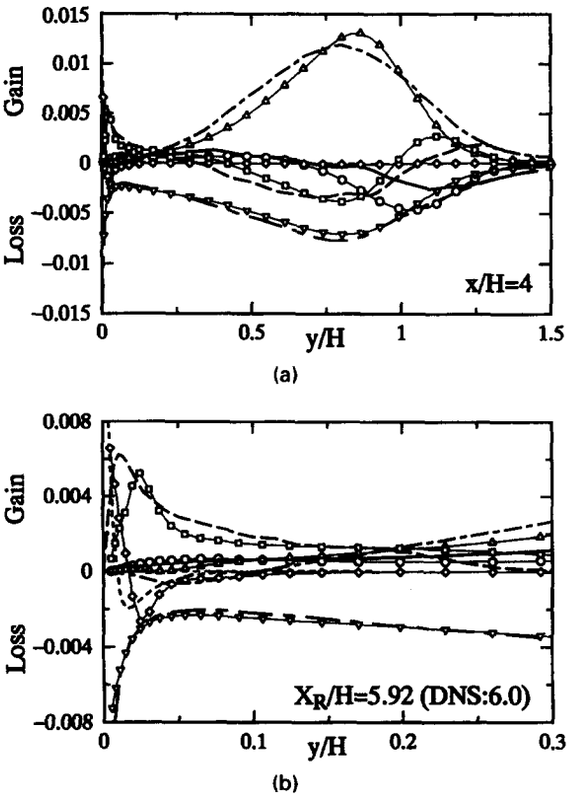

Figure 13 Budget of turbulent energy in backward-facing step flow at $x/H=4$ (case 1, normalized by $\overline{U}_0^3/H$, present model): convection -○- model, —— DNS; turbulent diffusion _□_ model, --- DNS; viscous diffusion _◇_ model, ---- DNS; production _△_ model, ------ DNS; dissipation _▽_ model, -·-DNS; (a) overall view; (b) close to wall on step side

Equations 23 and 24.

$$f_{t1} = 1 + 5.0\exp\left[-\left(\frac{n^*}{5}\right)^2\right], \qquad f_{t2} = 1 + 4.0\exp\left[-\left(\frac{n^*}{5}\right)^2\right] \tag{30}$$

These model functions f_{t1} and f_{t2} increase the turbulent diffusion in the vicinity of the wall. As a result, the turbulent energy budget of the DNS (Kim et al. 1990) (including the profile of the dissipation rate) can successfully be predicted, as shown later. The model functions and constants adopted in the present model are summarized in Table 1.

Relation between anisotropy tensors and velocity gradients

The capability of a turbulence model to accurately predict both wall-turbulent and homogeneous shear flows can be assessed by examining the relation between the anisotropy tensor b_{ij} and the shear component of the velocity gradient $\overline{U}_{1,2}$. The variations of b_{ij} with the shear parameter $\overline{U}_{1,2}k/\varepsilon$ are shown in Figure 1, in which the results by the Standard nonlinear model (Equation 15) and the model of Shih et al. (1994) (hereafter referred to as the SH model) are also included for comparison. The Reynolds stress of the SH model is expressed as follows:

$$\begin{aligned}\overline{u_i u_j} = {} & \frac{2}{3}k\delta_{ij} - \frac{2/3}{5.5 + \left(\frac{k}{\varepsilon}S\right)}\left(\frac{k^2}{\varepsilon}\right)\left(\overline{U}_{i,j} + \overline{U}_{j,i}\right) \\ & + \frac{1}{1000 + \left(\frac{k}{\varepsilon}S\right)^3 + \left(\frac{k}{\varepsilon}\Omega\right)^3}\left(\frac{k^3}{\varepsilon^2}\right) \\ & \times\left[-4\left(\overline{U}_{i,k}\overline{U}_{k,j} + \overline{U}_{j,k}\overline{U}_{k,i} - \frac{2}{3}\overline{U}_{m,n}\overline{U}_{n,m}\delta_{ij}\right)\right. \\ & + 13\left(\overline{U}_{i,k}\overline{U}_{j,k} - \frac{1}{3}\overline{U}_{m,n}\overline{U}_{m,n}\delta_{ij}\right) \\ & \left. - 2\left(\overline{U}_{k,i}\overline{U}_{k,j} - \frac{1}{3}\overline{U}_{m,n}\overline{U}_{m,n}\delta_{ij}\right)\right]\end{aligned} \tag{31}$$

Table 1 Model functions and model constants

Model	f_μ						
Present	$\{1+(35/R_t^{3/4})\exp[-(R_t/30)^{3/4}]\}\{1-\exp[-(n^*/26)^2]\}$						
Model	f_ε						
Present	$\{1-0.3\exp[-(R_t/6.5)^2]\}\{1-\exp[-(n^*/3.7)^2]\}$						
Model	f_{t1}			f_{t2}			
Present	$1+5\exp[-(n^*/5)^2]$			$1+4\exp[-(n^*/5)^2]$			
Model	C_μ	C_D	$C_{\varepsilon 1}$	$C_{\varepsilon 2}$	C_s	C_ε	C_η
Present	0.12	0.8	1.45	1.9	1.4	1.4	5.0

$[n^* = (u_\varepsilon n/\nu),\ R_t = (k^2/\nu\varepsilon)]$

where S and Ω are the invariants of the strain-rate and vorticity tensors, respectively; i.e., $S = (2S_{mn}S_{mn})^{1/2}$ and $\Omega = (2\Omega_{mn}\Omega_{mn})^{1/2}$. Note that, in Figure 1, the terms WTF and HSF denote, respectively, wall-turbulent ($P_k/\varepsilon = 1$) and homogeneous shear [$P_k/\varepsilon = (C_{\varepsilon 2} - 1)/(C_{\varepsilon 1} - 1)$] flows. It can be seen that the present model (Equation 21) successfully reproduces both wall-turbulent and homogeneous shear flows compared with the Standard model (Equation 15) as shown in Figure 1a, where the experimental data on HSF were compiled by Tavoularis and Corrsin (1981). Because the relationship between the anisotropy tensor b_{12} and the shear parameter $\overline{U}_{1,2}k/\varepsilon$ in the Standard model (Equation 15) is linear, it cannot essentially predict wall-turbulent and homogeneous shear flows simultaneously, where b_{12} in both situations are almost equal ($\simeq -0.15$) for the different values of $\overline{U}_{1,2}k/\varepsilon$. We can also understand from Figure 1b that the accuracy of the present model is better than that of the SH model, because the latter shows some discrepancies even in the WTF region. These discrepancies usually cannot be overlooked in this type of two-equation model.

As already mentioned, unreasonable results with negative turbulent intensities occur in the condition of $S^{*2} \gg \Omega^{*2}/4$, in which the normal component of the velocity gradient $\overline{U}_{1,1}$ (i.e., elongation or contraction) is dominant. Figure 2 shows a comparison among the variations of b_{ij} with $\overline{U}_{1,1}k/\varepsilon$ obtained by the original model (Equation 11), the Padé model (Equation 17), the SH model (Equation 31) and the present model (Equation 21). It can easily be understood that unacceptable negative turbulent intensities are obtained by the original and Padé models, although the Padé-type modification considers the positiveness of the coefficient in Equation 11 as previously described. On the other hand, the present and SH models give non-negative turbulent intensities. Moreover, in marked contrast to the SH model, the behavior of the present model is quite similar to that of the

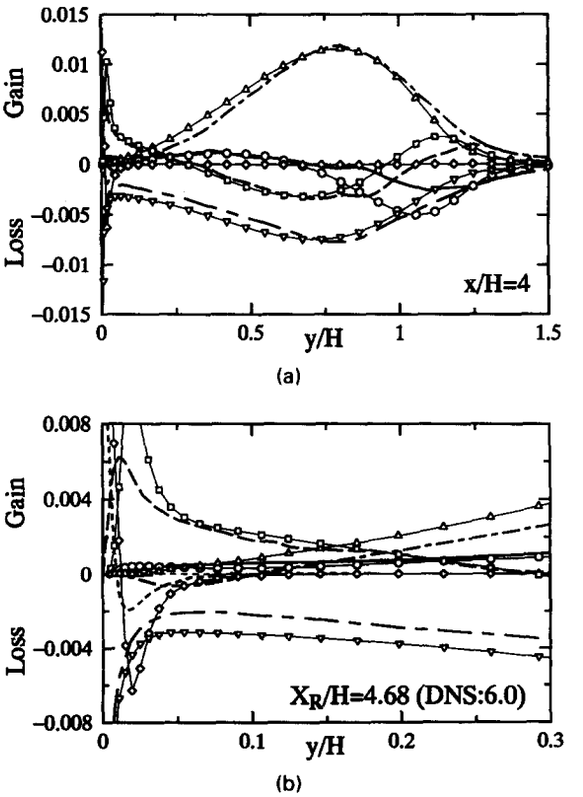

Figure 14 Budget of turbulent energy in backward-facing step flow at $x/H = 4$ (YS1 model, key as Figure 13): (a) overall view; (b) close to wall on step side

original model in the region of $\overline{U}_{1,1}k/\varepsilon < 3$. As seen from Figures 1b and 2, the anisotropy predicted by the SH model is much weaker than that by the present model, which results in a difference of accuracy in predicting homogeneous shear flow, as shown later.

Numerical procedure

All the following calculations were performed using the finite difference method except for homogeneous shear flow which was calculated using a simple algorithm by the Runge–Kutta method. The generalized coordinate system was employed, which consists of ξ- and η-coordinates. The primitive variables, $\overline{U}_i$, k, and ε, were colocated; whereas, the pressure was located in a staggered position (Kuno et al. 1992). We adopted the third-order upwind difference for the convection term in Equation 2, the first-order upwind difference for the convection terms in Equations 3 and 4, and the second-order central difference for the other terms. Note that the influence of numerical viscosity attributable to the first-order upwind difference in Equations 3 and 4 was not significant, because the budgets of k and ε were dominated by the production and destruction terms in the flow fields examined in this study. Furthermore, calculations with several different grid points were conducted, and we confirmed that grid-independent solutions could be obtained. Details of the computational procedure are described in Abe et al. (1994; 1995), which also include discussions on grid dependence.

Three of the other LRN k-ε models were selected for comparison; i.e., two types of models recently proposed by Yang and Shih [hereafter referred to as the YS1 model (Yang and Shih 1993a) and the YS2 model (Yang and Shih 1993b)] and the model by Launder and Sharma [hereafter referred to as the LS model (Launder and Sharma 1974; Chieng and Launder 1980)]. These are summarized in Table 2, where the transport equations of k and ε are expressed as follows:

$$\frac{Dk}{Dt} = \frac{\partial}{\partial x_j}\left\{\left(\nu + \frac{\nu_t}{\sigma_k}\right)\frac{\partial k}{\partial x_j}\right\} - \overline{u_i u_j}\frac{\partial \overline{U}_i}{\partial x_j} - (\varepsilon + D), \tag{32}$$

$$\frac{D\varepsilon}{Dt} = \frac{\partial}{\partial x_j}\left\{\left(\nu + \frac{\nu_t}{\sigma_\varepsilon}\right)\frac{\partial \varepsilon}{\partial x_j}\right\} - C_{\varepsilon 1} f_1 \frac{\varepsilon}{k}\overline{u_i u_j}\frac{\partial \overline{U}_i}{\partial x_j} - C_{\varepsilon 2} f_2 \frac{\varepsilon^2}{k} + E \tag{33}$$

Table 2 Model functions and model constants

Model	f_μ
YS1	$[1+(1/R_t^{1/2})][1-\exp(-a_1 n_k - a_3 n_k^3 - a_5 n_k^5)]^{1/2}$
YS2	$[1+(1/R_t^{1/2})][1-\exp(-b_1 R - b_2 R^2 - b_3 R^3)]^{1/2}$
LS	$\exp[-3.4/(1+R_t/50)^2]$

Model	f_1	f_2
YS1	$R_t^{1/2}/(R_t^{1/2}+1)$	$R_t^{1/2}/(R_t^{1/2}+1)$
YS2	$R_t^{1/2}/(R_t^{1/2}+1)$	$R_t^{1/2}/(R_t^{1/2}+1)$
LS	1	$1-0.3\exp(-R_t^2)$

Model	C_μ	σ_k	σ_ε	$C_{\varepsilon 1}$	$C_{\varepsilon 2}$	D	E
YS1	0.09	1.0	1.3	1.44	1.92	0	$\nu\nu_t(\overline{U}_{i,jk})^2$
YS2	0.09	1.0	1.3	1.44	1.92	0	$\nu\nu_t(\overline{U}_{i,jk})^2$
LS	0.09	1.0	1.3	1.44	1.92	$2\nu(k_{,j}^{1/2})^2$	$2\nu\nu_t(\overline{U}_{i,jk})^2$

$[n_k = k^{1/2}n/\nu,\ R = k/\nu S,\ R_t = k^2/\nu\varepsilon,\ (a_1, a_3, a_5) = (1.5\times10^{-4},\ 5\times10^{-7},\ 1\times10^{-10}),\ (b_1, b_2, b_3) = (3\times10^{-4},\ 6\times10^{-5},\ 2\times10^{-6})]$

with

$$-\overline{u_i u_j} = C_\mu f_\mu \frac{k^2}{\varepsilon}\left(\frac{\partial \overline{U}_i}{\partial x_j} + \frac{\partial \overline{U}_j}{\partial x_i}\right) - \frac{2}{3}k\delta_{ij} \tag{34}$$

Note that $R(=k/\nu S)$ used in the YS2 model is a recently proposed parameter with no reference to the distance from the wall (Yang and Shih 1993b).

Model assessment in basic turbulent flows

To confirm the basic accuracy of the present model, we applied it to two representative turbulent flows; i.e., homogeneous shear flow corresponding to the experiment by Tavoularis and Corrsin (1981) and channel flow corresponding to the DNS by Kim et al. (1990).

Variations of the Reynolds shear stress in the homogeneous shear flow are shown in Figure 3. Results by the Standard nonlinear model (Equation 15) and the SH model (Equation 31) are also included. From Figure 3, it is clear that accuracy in calculating homogeneous shear flow is dramatically improved by the present model. The comparison of the anisotropy is shown in Figure 4. The computational results of the present model agree well with the experimental data; whereas, the SH model shows considerably weak anisotropy. The SH model does not take into

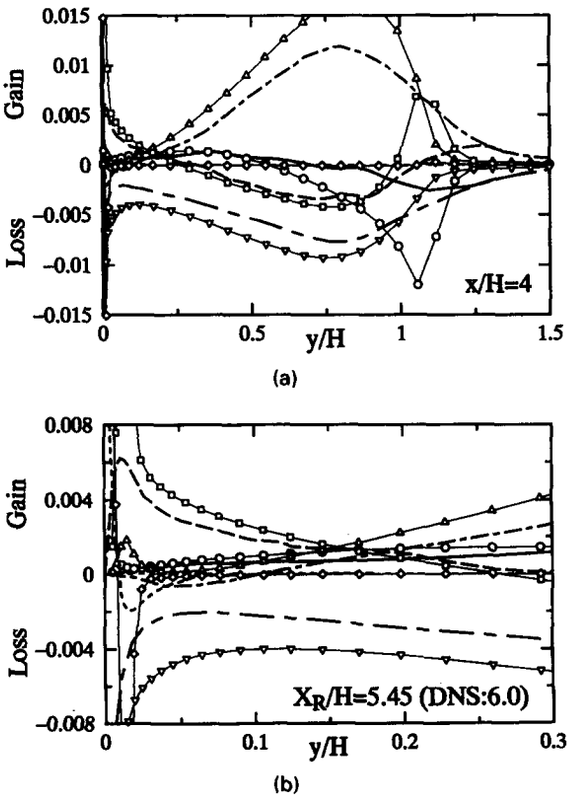

Figure 15 Budget of turbulent energy in backward-facing step flow at $x/H = 4$ (YS2 model, key as Figure 13): (a) overall view; (b) close to wall on step side

account compatibility with higher-order closure models. This seems to explain the difference in accuracy between the present and SH models.

Figures 5 and 6 show the results of the channel flow with the present model calculated under the DNS condition. In Figure 5, two types of grid points are tested to examine grid dependence; i.e., 151 and 301. The Reynolds number based on the friction velocity u_τ and the half-width of the channel δ was $\mathrm{Re}_\tau = u_\tau \delta/\nu = 395$. From Figure 5a, we can see that almost perfect grid-independent solutions are obtained in the calculations. Also, from Figures 5 and 6, it can be seen that the mean velocity, turbulent energy, Reynolds shear stress, and dissipation rate are quite successfully predicted, and that all terms of the turbulent energy budget are in good agreement with the DNS data (Figure 6). The accuracy of the mean-velocity results is validated in a wide range of the Reynolds numbers, as shown in Figure 7.

Application to complex turbulent flows

Channel flow with injection and suction

The introduction of flow injection and suction is one of the most important strategies to control turbulent flows and heat transfer. It is well known that even a small amount of mass injection and suction (only about 0.3% of the bulk-flow rate) greatly influences the turbulent structures (Sumitani and Kasagi 1995). Thus, the present model was applied to this type of turbulent flow to assess the accuracy in the flows with complex boundary conditions. Two types of flow conditions were considered. One was uniform injection at one wall and uniform suction at the same rate at the other wall corresponding to the DNS by Sumitani and Kasagi.

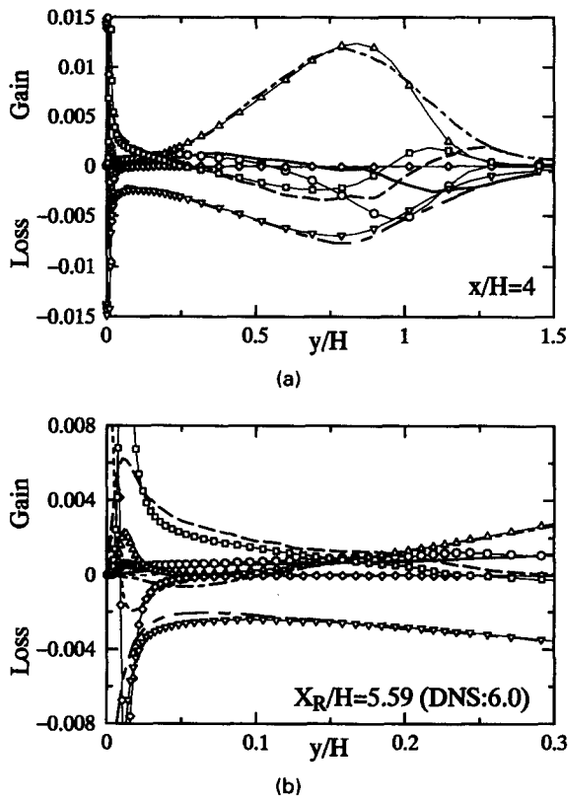

Figure 16 Budget of turbulent energy in backward-facing step flow at $x/H = 4$ (LS model, key as Figure 13): (a) overall view; (b) close to wall on step side

The other was periodic injection and suction at one side wall corresponding to the DNS by Miyake et al. (1995). The latter case seems particularly difficult to predict accurately, because a periodic change in pressure gradient is induced by flow injection and suction, so that the flow field may show characteristics of both favorable and adverse pressure gradient flows (Miyake et al.).

Concerning the former test case of Sumitani and Kasagi (1995), the Reynolds number based on the averaged friction velocity on both side walls u_τ^{**} and the half-width of the channel δ was $\mathrm{Re}_\tau = u_\tau^{**}\delta/\nu = 150$, and the injection and suction velocity was set to $\bar{V}/u_\tau^{**} = 0.05$. The calculation was conducted with the grid points of 101. Profiles of the mean velocity and Reynolds shear stress are shown in Figure 8, and skin friction coefficients C_f are shown in Table 3, in which $(\ )^+$ denotes the values normalized by friction velocity on each side wall, and $(\ )^{**}$ are those normalized by the averaged friction velocity u_τ^{**}. The results for channel flow without any injection and suction corresponding to the DNS of Kuroda et al. (1993) (hereafter referred to as the Normal case) are also included for comparison. These data make it clear that the present model has the capability to accurately predict the mean velocity, Reynolds shear stress, and friction coefficient. The budgets of turbulent energy are shown in Figure 9. It can be seen that all the terms of the budget on the injection side are accurately predicted; whereas, those on the suction side show some discrepancies with the DNS data. This issue needs more detailed study in the future.

As for the latter test case of Miyake et al. (1995) with a periodic change in pressure gradient, the Reynolds number was $\mathrm{Re}_\tau = u_\tau^{**}\delta/\nu = 150$, and the injection and suction velocity was set to $\bar{V}/u_\tau^{**} = -0.5\sin(2\pi x/L)$ at one side wall, where $L(= 4\pi\delta)$ was the length of one period of injection and suction. The number of grid points was 185×101. The variations in mean velocity obtained from the present model and three LRN models; i.e., YS1, YS2, and LS, are shown in Figure 10. In this type of flow field, the mean-velocity profile shifts up and down across the line of the log-law according to the mean-pressure gradient. The mean-velocity profiles of the present and YS1 models give reasonable overall predictions, although there exist some discrepancies in the amplitude of the shift across the log-law line. On the other hand, the YS2 and LS models show considerable overpredictions at $x = 5L/8$ and $6L/8$. It seems that the LRN parameters adopted in the model functions account for the difference in computational accuracy. This issue is discussed in detail in the later section.

Backward-facing step flow

To validate the accuracy in complex separated and reattaching turbulent flows, we applied the present model to the flows downstream of a backward-facing step. The calculations were conducted corresponding to five experimental cases, as shown in Table 4.

The reattachment lengths X_R obtained from the computational results are shown in Table 5 with the corresponding experimental data. From Table 5, we can understand how the present model can successfully predict the reattachment lengths of the backward-facing step flows over a wide range of the expansion ratio and Reynolds number.

Table 3 Skin-friction coefficient C_f in the channel flow with injection and suction

	Normal	Injection side	Suction side
Prediction	8.85×10^{-3}	6.40×10^{-3}	1.31×10^{-2}
DNS	8.64×10^{-3}	6.29×10^{-3}	1.27×10^{-2}

Table 4 Computational conditions for back-step flows

	Case 1, Le et al. (1993)	Case 2, Vogel and Eaton (1985)	Case 3, Kasagi and Matsunaga (1995)
ER	1.2	1.25	1.5
Re_H	5100	28000	5500
Re_θ	700	4500	500
θ/H	0.14	0.16	0.09
$N_\xi \times N_\eta$	389 × 145	325 × 125	303 × 125

	Case 4, Eaton and Johnston (1980)	Case 5, Durst and Schmitt (1985)
ER	1.67	2.0
Re_H	38000	100000
Re_θ	1200	4000
θ/H	0.03	0.04
$N_\xi \times N_\eta$	341 × 111	359 × 125

Table 5 Comparison of flow reattachment lengths, X_R/H

	Case 1	Case 2	Case 3	Case 4	Case 5
Prediction	5.9	6.4	6.6	8.1	8.7
Experiment	6.0	6.7	6.5	8.0	8.4

The streamlines and the skin friction coefficient in case 2 obtained by the present model are shown in Figure 11. The accuracy of the skin friction coefficient in the recirculating region is considerably improved compared with the linear k-ε model of Abe et al. (1994). A comparison of the computational results with the experiment of Kasagi and Matsunaga (1995) (case 3) is shown in Figure 12, in which predictions by the present model are in good agreement with the experimental data. The turbulent energy budgets at $x/H = 4$ in case 1, obtained by the present model and three LRN models listed in Table 2, are shown in Figures 13–16. We can definitely declare from these figures that the present model gives the best predictions, as compared with the other three models, all of which considerably overpredict the molecular diffusion, turbulent diffusion, and dissipation rate in the near-wall region. Note that, in these models, the total dissipation rate is estimated as $\varepsilon_{\text{total}} = \varepsilon + D$, where D is the extra term in Equation 32 defined in Table 2. Furthermore, predictions by the YS2 and LS models show the spiky behavior of the production term in the immediate vicinity of the wall, which is in conflict with the DNS data of Le et al. (1993). It is also suggested that the LRN parameters adopted in the model functions greatly influence the computational results (details are discussed in the next section).

Examination of low-Reynolds-number parameters in model functions

Recently, many types of LRN k-ε models have been proposed in which various types of LRN parameters were adopted; e.g., $n^* = u_\varepsilon n/\nu$, $R_t = k^2/\nu\varepsilon$, $n_k = k^{1/2}n/\nu$, $R = k/\nu S$, and so on. It is usually said that the LRN parameters without the wall distance are desirable for a more general purpose LRN k-ε model (Yang and Shih 1993b). Most of the proposed models without the wall distance have, however, been applied only to relatively simple flow fields for the assessment of accuracy; whereas, these models were constructed for application to complex turbulent flows as represented by flows with injection, suction, and separation. Furthermore, as revealed by the above discussions, the LRN parameters adopted in the model functions show considerable difference in the accuracy of flow-field prediction. In this section, therefore, we investigate the characteristics of the LRN parameters in complex turbulent flows based on the computational results previously obtained.

First, based on the computational results shown in Figure 10 and Figures 13–16, the examined models can be divided by whether or not their predictions reasonably agree with the experimental and DNS data. One group consists of the present and YS1 models, and the other of the YS2 and LS models. It is the former group that gives reasonable predictions for both the channel flow with periodic injection and suction, and the backward-facing step flow. This grouping coincides with whether or not the wall distance n is included in the model functions, as shown in Tables 1 and 2. *In other words, the LRN parameters in the latter group consist of two or more turbulent characteristics.*

Streamwise variations in turbulent characteristics at the locations of $y/\delta = 1/3$ and $1/5$ in the channel flow with periodic injection and suction are shown in Figures 17 and 18, respectively, in which all variables are normalized by the value averaged in the streamwise direction at that y location. It can be seen that the behavior of $k^{1/2}$ and u_ε is quite similar, as shown in Figures 17a and b; whereas, R_t shows a different variation whose phase shifts by about π from $k^{1/2}$ and u_ε. This is a novel feature since R_t consists of $k^{1/2}$ and u_ε; i.e., $R_t = k^2/\nu\varepsilon = (k^{1/2}/u_\varepsilon)^4$. A slight difference in the variations between $k^{1/2}$ and u_ε may be amplified in R_t by the fourth power relation which can cause anomalous behavior. This phase shift can also be observed in Figures 17c and d, in which a more definite discrepancy appears between the above variables. Furthermore, it is worth noting that, among all variables shown in Figure 17, only R shows a different behavior in the two groups mentioned above. In particular, the prediction of R by the YS2 model (Figure 17c) shows a tendency similar to that of R_t by the LS model (Figure 17d), which may lead to similar predictions of the mean- and friction-velocity profiles. These findings also apply to the location of $y/\delta = 1/5$, as shown in Figure 18, except that the behavior of R in two groups becomes more similar than that at $y/\delta = 1/3$. From these discussions, it can be more readily seen that the LRN parameters; e.g., $R_t = k^2/\nu\varepsilon$, constructed by two or more turbulent characteristics; i.e., k, ε and so on, may result in unexpected behavior because of an amplification of the difference between

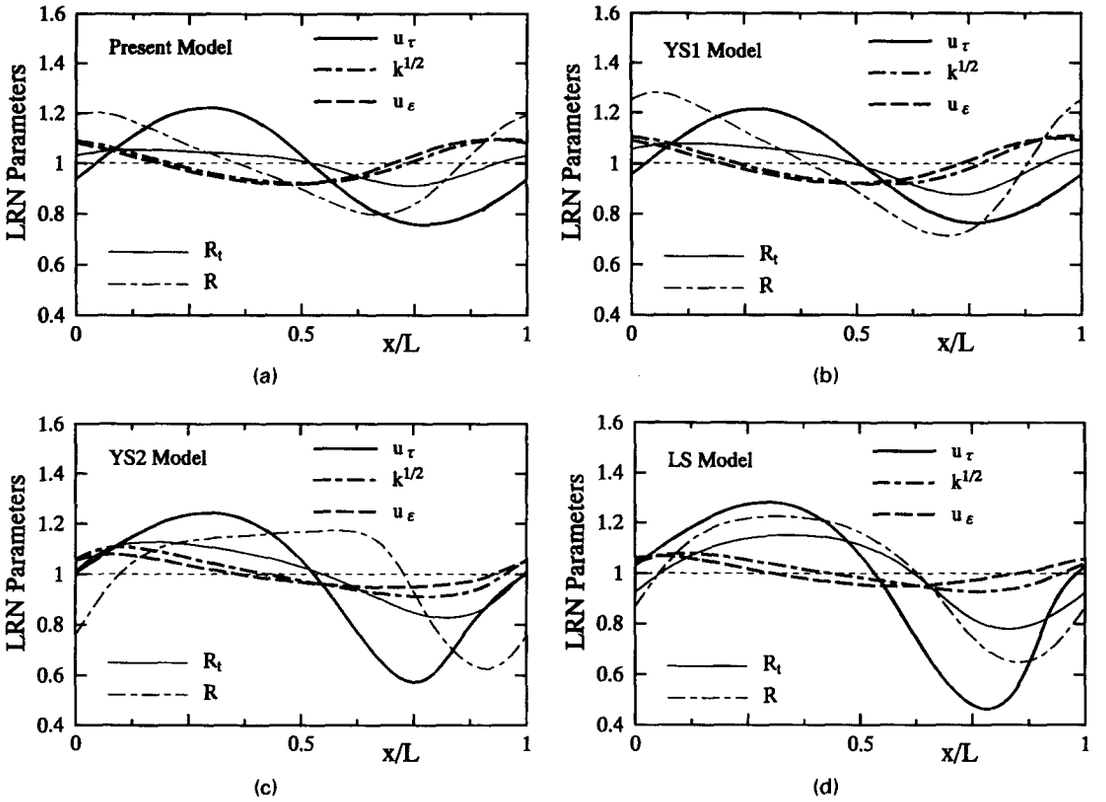

Figure 17 Turbulent characteristics in channel flow with periodic injection and suction at one side wall ($y/\delta = 1/3$): (a) present model; (b) Yang–Shih (YS1) model; (c) Yang–Shih (YS2) model; (d) Launder–Sharma (LS) model

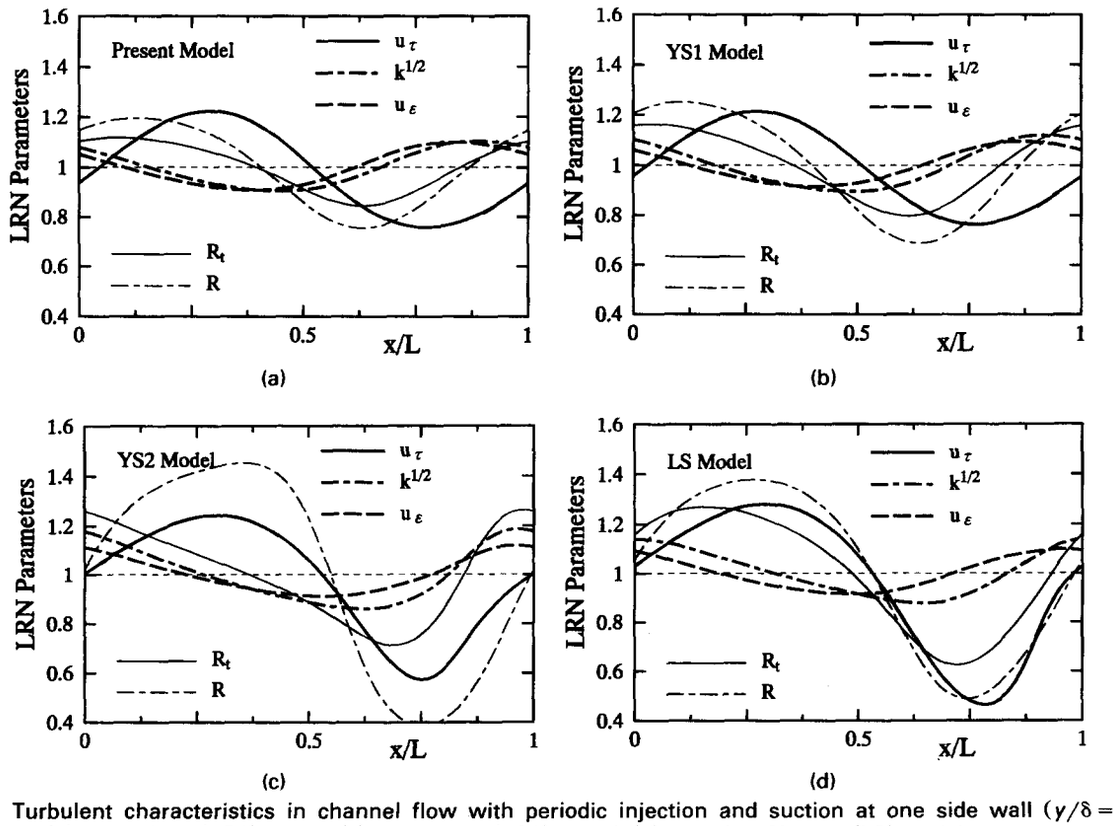

Figure 18 Turbulent characteristics in channel flow with periodic injection and suction at one side wall ($y/\delta = 1/5$): (a) present model; (b) Yang–Shih (YS1) model; (c) Yang–Shih (YS2) model; (d) Launder–Sharma (LS) model

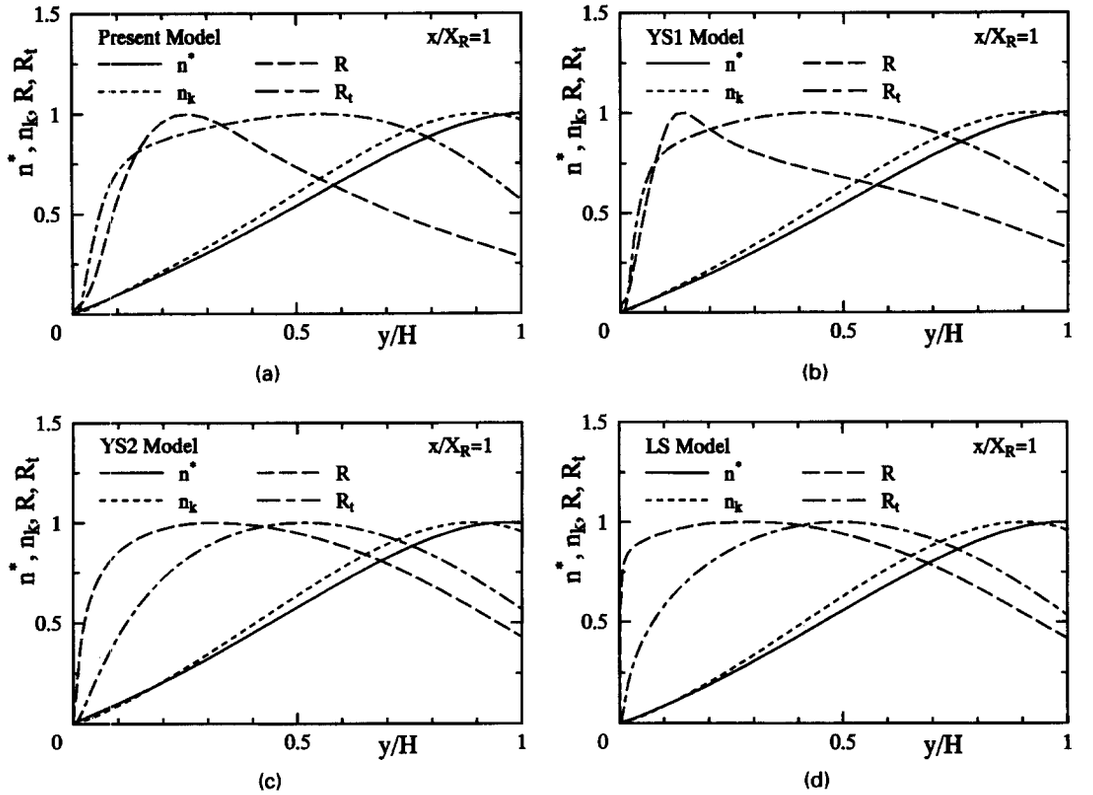

Figure 19 Turbulent characteristics in backward-facing step flow (case 1, $x/X_R = 1$): (a) present model; (b) Yang–Shih (YS1) model; (c) Yang–Shih (YS2) model; (d) Launder–Sharma (LS) model

the variations in turbulent characteristics. We can also understand that the phase of a near-wall scaling parameter greatly influences the prediction accuracy for complex turbulent flows.

The cross streamwise variations in turbulent characteristics in the backward-facing step flow of case 1 at the reattachment point, $x/X_R = 1$, are shown in Figure 19, in which all variables are normalized by the maximum value in the section. It is clear that R and R_t rapidly increase in the immediate vicinity of the wall and decrease before the step-height location of $y/H = 1$. This kind of behavior is undesirable as a scaling parameter in the near-wall region. The rapid increase in LRN parameters results in a thinning of the viscous sublayer. Launder (1988) indicates that the LS model using R_t gives an immoderate thinning of the viscous sublayer and an excessively large turbulent length scale near the reattachment point in separating flows, which leads to an unacceptable overprediction of the heat transfer coefficient. On the other hand, as discussed in the previous studies (Abe et al. 1994; 1995), parameters such as u_τ and R constructed by the mean-velocity gradient pose a problem at the separating and reattaching points, where the near-wall limiting behavior of Reynolds shear stress given by the models using these parameters changes along with change in that of the mean velocity; i.e., $\overline{U} \propto n^2$ for $n \to 0$. In addition, parameters with the mean-velocity gradient do not seem to be essential for flow regions where the production term of turbulent energy is relatively small compared with the other terms; e.g., the shear-free side in Couette–Poiseuille flows and the recirculating region in separating flows. In such flow fields, turbulent diffusion is usually the dominant term on the gain side of the turbulent energy budget (Abe et al. 1995; Le et al. 1993). Thus, the inclusion of R in the model functions is not always reasonable where complex turbulent flows are concerned.

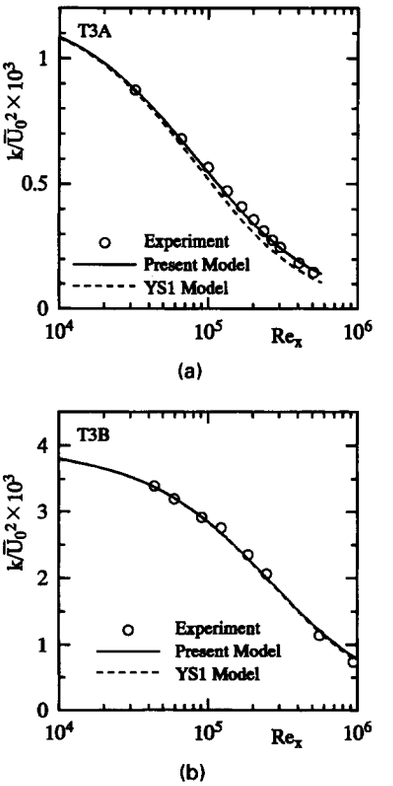

Figure 20 Streamwise variations of turbulent energy in free-stream region: (a) T3A case; (b) T3B case

In sum, the following knowledge emerged from the present investigation. First, the turbulent Reynolds number $R_t = k^2/\nu\varepsilon$, and the recently proposed parameter $R = k/\nu S$, neither of which include the distance from the wall, are inapplicable to some complex turbulent flows. Second, the essential difficulty in constructing the LRN parameter without the wall distance n seems to lie in the necessity of two or more turbulent characteristics. Third, the combination of two or more turbulent characteristics; e.g., $R_t = k^2/\nu\varepsilon$, could result in characteristics quite different from the original ones, even if their profiles show a similar tendency in the flow field.

Bypass transition

The prediction of bypass (or diffusion-controlled) transition is another interesting concern from the engineering viewpoint. Therefore, to assess the model performance in such transitional flows, we applied the present model to some test cases of bypass transition.

So far, most calculations have been made with the parabolic computational procedure, mainly because of the computational cost. Recently, however, some problems have been pointed out regarding the initial and boundary conditions in the parabolic calculations. Craft et al. (1996) and Suga (1996) argued that elliptic computations from the uniform region upstream of the leading edge are effective to exclude ambiguities in the initial and boundary conditions. With this in mind, the present calculations were conducted with the same elliptic computational procedure as in the calculations of backward-facing step flows.

Two test cases are selected. One is the bypass transition on a flat plate under the influence of free-stream turbulence of 3%, and the other is that of 6% (hereafter referred to as T3A and T3B, respectively) (Savill 1993). Calculations by the YS1 model were also performed for comparison. This model is now regarded as one of the most advanced models using the LRN parameter $n_k = k^{1/2}n/\nu$ (the previous representative being the model of Lam and Bremhorst 1981). Concerning the computational domain, grid resolution, and boundary conditions, we basically followed the procedures of Craft et al. (1996) and Suga (1996). The number of grid points was 173×121, and the first grid points from the wall were located at $y^+ < 1.0$, except the point at the leading edge ($y^+ \simeq 1.3$). Turbulent energy and dissipation rate at the inlet position upstream of the leading edge were specified so as to faithfully reproduce the experimental data of turbulent energy decaying in the free stream. The predicted variations of the free-stream turbulence are shown in Figure 20, in which excellent agreement with the experimental data is indicated. This also demonstrates the validity of the inlet conditions specified in this study.

The predicted skin friction coefficients are compared with the experimental data in Figure 21, and the corresponding variations of the shape factor are shown in Figure 22. The present model gives predictions much better than the YS1 model, although both models give earlier transition than that seen in the experiments. Profiles of the mean velocity, turbulent energy, and Reynolds shear stress are shown in Figures 23–25, respectively. From these figures, it can also be seen that the predictions by the present model are better than those by the YS1 model. However, some discrepancies exist between the predictions and the experimental data, mainly caused by the difference in predicting the transition point. Savill (1993) stated that LRN models using the wall distance (e.g., y^+ and n_k) in the model functions predict earlier transition points than the experiments and the LS model is still one of the best models for the prediction of transition points. In general, within the framework of two-equation modeling, accurate calculations of all the turbulent characteristics in the bypass

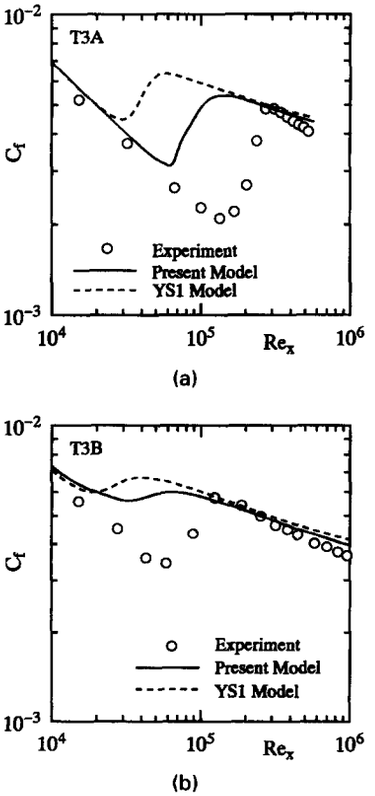

Figure 21 Streamwise variations of skin friction coefficient: (a) T3A case; (b) T3B case

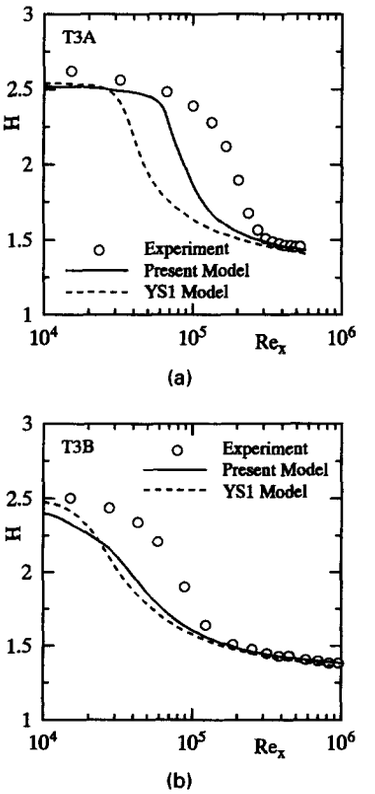

Figure 22 Streamwise variations of shape factor: (a) T3A case; (b) T3B case

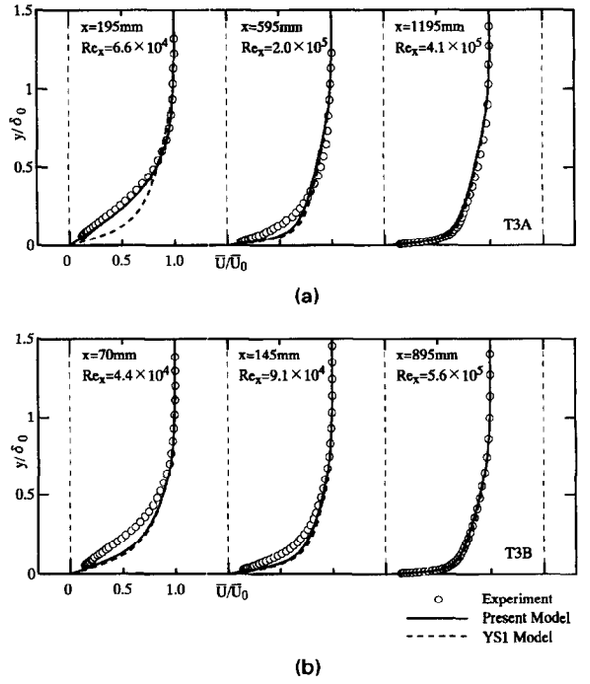

Figure 23 Profiles of mean velocity: (a) T3A case; (b) T3B case

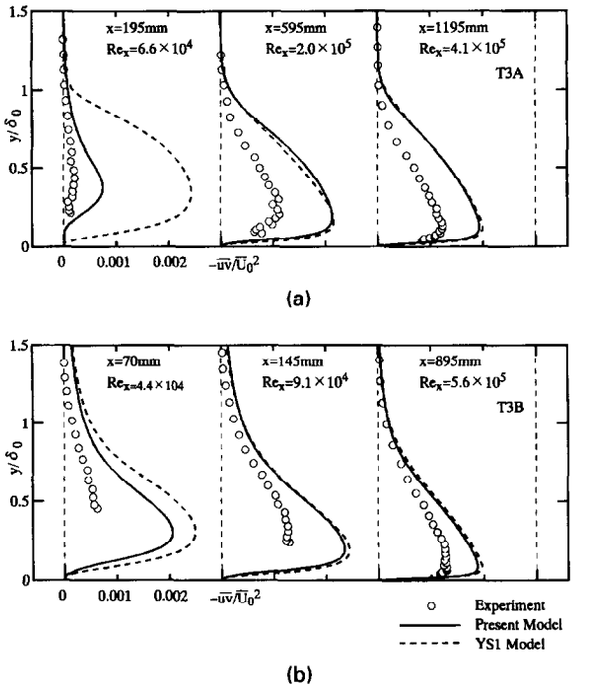

Figure 25 Profiles of Reynolds shear stress: (a) T3A case; (b) T3B case

transition regime are very difficult, especially the variations of both k and $\overline{uv}$. It is clear from the experiments that, in the region near the transition point, the Reynolds shear stress $\overline{uv}$ in the boundary layer is very small; whereas, the turbulent energy (or turbulent intensity) has a larger level, which results in a very small value of the structure parameter (or b_{12}). It is known that the LS model predicts the more reasonable transition points for both T3A and T3B cases (Craft et al. 1996; Suga 1996). In the region near the transition point, however, the turbulent energy predicted by the LS model is too small to coincide with experimental knowledge. As shown previously, not only the YS1 model but also the present model cannot accurately predict these phenomena. In contrast to the LS model, the turbulent energy profiles predicted by the present model are in global agreement with the experimental data in the region near the transition point. Yet, the Reynolds shear stress is overpredicted, which would lead to earlier predictions for the transition point.

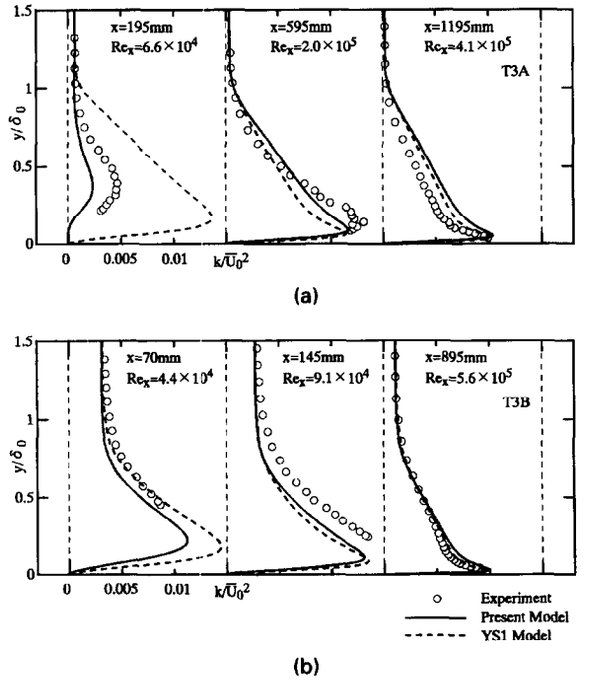

Figure 24 Profiles of turbulent energy: (a) T3A case; (b) T3B case

From the above investigations, it can be seen that even the present model does not have the capability to predict all the turbulent characteristics in transitional flows sufficiently. This difficulty arises from the fact that, to predict bypass transition accurately, any turbulence model has to predict a very low level of the structure parameter in the region near the transition point, a fact that is not considered sufficiently in the basic concept of two-equation modeling. As for the prediction of a transition point, the LS model may still be useful. As already demonstrated, however, it is also true that the LRN parameter R_t used in the LS model has some difficulties in predicting the flow fields with pressure gradient and/or separation, where the flow is fully turbulent. To improve the prediction accuracy for transitional flows, while maintaining the advantages of the present model for fully turbulent flows, more detailed investigations are needed.

Conclusions

We have proposed a new type of k-ε model that incorporates some essential characteristics of second-order closure models. The present model is suitably extended to an LRN k-ε model by introducing the Kolmogorov velocity scale to reproduce near-wall limiting behavior and to allow application to complex turbulent flows with separation and reattachment.

The calculations show that the present model is capable of predicting both wall-turbulent and homogeneous shear flows. In

channel flows with injection and suction at wall surfaces, and separated and reattaching flows downstream of a backward-facing step, the comparison of computational results with the experimental and DNS data indicates that the present model is also effective in calculating complex turbulent flows of technological interest.

Furthermore, in this study, we have reexamined the parameters adopted in the LRN model functions based on a comparison of computational results by the present model with those of several LRN k-ε models previously proposed. From this investigation, several insights are obtained. In particular, it is shown that the use of LRN parameters constructed by two or more turbulent characteristics poses some difficulties for application to complex turbulent flows. For example, the LRN models using $R_t(=k^2/\nu\varepsilon)$ and $R(=k/\nu S)$ examined in this study show considerable discrepancies with the experimental and DNS data, in spite of being generally regarded as effective LRN parameters, because they do not include the distance from the wall. Most of the recent research focusing on this issue only combines the turbulent quantities in constructing near-wall scaling parameters to exclude the wall distance, but there has been little discussion as to the physical meaning of the asymptotic expression, including all model functions. *From the practical viewpoint, further efforts to develop a new scaling parameter without the wall distance are needed. However, careful and detailed discussions on the physics of turbulence in the near-wall region should be made in constructing a new scaling parameter.*

References

Abe, K., Kondoh, T. and Nagano, Y. 1994. A new turbulence model for predicting fluid flow and heat transfer in separating and reattaching flows—I. Flow-field calculations. *Int. J. Heat Mass Transfer*, **37,** 139–151

Abe, K., Kondoh, T. and Nagano, Y. 1995. A new turbulence model for predicting fluid flow and heat transfer in separating and reattaching flows—II. Thermal field calculations. *Int. J. Heat Mass Transfer*, **38,** 1467–1481

Chieng, C. C. and Launder, B. E. 1980. On the calculation of turbulent heat transport downstream from an abrupt pipe expansion. *Numer. Heat Transfer*, **3,** 189–207

Craft, T. J., Launder, B. E. and Suga, K. 1996. The prediction of turbulent transitional phenomena with a nonlinear eddy-viscosity model. *Proc. Engineering Foundation Conference on Turbulent Heat Transfer*, San Diego, CA

Daly, B. J. and Harlow, F. H. 1970. Transport equations in turbulence. *Phys. Fluids*, **13,** 2634–2649

Durst, F. and Schmitt, F. 1985. Experimental studies of high Reynolds number backward-facing step flow. *Proc. 5th Symposium on Turbulent Shear Flows*, 5.19–5.24

Eaton, J. K. and Johnston, J. P. 1980. Turbulent flow reattachment: An experimental study of the flow and structure behind a backward-facing step. MD-39, Thermosciences Division, Department of Mechanical Engineering, Stanford University, Stanford, CA

Gatski, T. B. and Speziale, C. G. 1993. On explicit algebraic stress models for complex turbulent flows. *J. Fluid Mech.*, **254,** 59–78

Kasagi, N. and Matsunaga, A. 1995. Three-dimensional particle-tracking velocimetry measurement of turbulence statistics and energy budget in a backward-facing step flow. *Int. J. Heat Fluid Flow*, **16,** 477–485

Kim, J. et al. 1990. The collaborative testing of turbulence models (organized by P. Bradshaw et al.), data disk no. 4

Kline, S. J. et al. 1981. *Proc. 1980–81 AFOSR-HTTM-Stanford Conference on Complex Turbulent Flows: Comparison of Computation and Experiment I, II and III*, Stanford University, Stanford, CA

Kuno, T., Satofuka, N. and Tokunaga, H. 1992. Numerical solution of incompressible flow of power-law fluid using boundary-fitted curvilinear coordinates. *Trans. Japan. Soc. Mech. Eng.: Ser. B*, **58,** 2442–2448

Kuroda, A., Kasagi, N. and Hirata, M. 1993. Direct numerical simulation of turbulent plane Couette-Poiseuille flows: Effect of mean shear on the near wall turbulence structures. *Proc. 9th Symposium on Turbulent Shear Flows*, 8.4.1–8.4.6

Lam, C. K. G. and Bremhorst, K. 1981. A modified form of the k-ε model for predicting wall turbulence. *J. Fluids Eng.*, **103,** 456–460

Launder, B. E. 1988. On the computation of convective heat transfer in complex turbulent flows. *J. Heat Transfer*, **110,** 1112–1128

Launder, B. E., Reece, G. J. and Rodi, W. 1975. Progress in the development of a Reynolds-stress turbulence closure. *J. Fluid Mech.*, **68,** 537–566

Launder, B. E. and Sharma, B. I. 1974. Application of the energy-dissipation model of turbulence to the calculation of flow near a spinning disc. *Lett. Heat Mass Transfer*, **1,** 131–138

Le, H., Moin, P. and Kim, J. 1993. Direct numerical simulation of turbulent flow over a backward-facing step. *Proc. 9th Symposium on Turbulent Shear Flows*, 13.2.1–13.2.5

Miyake, Y., Tsujimoto, K., and Beppu, H. 1995. Direct numerical simulation of a turbulent flow in a channel having periodic pressure gradient. *Int. J. Heat Fluid Flow*, **16,** 333–340

Myong, H. K. and Kasagi, N. 1990. A new approach to the improvement of k-ε turbulence model for wall-bounded shear flows. *Int. J. Japan. Soc. Mech. Engs., Ser. II*, **33,** 63–72

Nagano, Y. and Shimada, M. 1995. Rigorous modeling of dissipation-rate equation using direct simulations. *Int. J. Japan. Soc. Mech. Eng., Ser. II*, **38,** 51–59

Nagano, Y. and Tagawa, M. 1990. An improved k-ε model for boundary-layer flows. *J. Fluids Eng.*, **112,** 33–39

Pope, S. B. 1975. A more general effective-viscosity hypothesis, *J. Fluid Mech.*, **72,** 331–340

Savill, A. M. 1993. Some recent progress in the turbulence modelling of by-pass transition. In *Near-Wall Turbulent Flows*, R. M. C. So, C. G. Speziale and B. E. Launder (eds.), Elsevier, New York, 829–848

Shih, T. H., Zhu, J. and Lumley, J. L. 1994. Modeling of wall-bounded complex flows and free shear flows. NASA TM 106513

Speziale, C. G. 1987. On nonlinear k-l and k-ε models of turbulence. *J. Fluid Mech.*, **178,** 459–475

Suga, K. 1996. Development and application of a nonlinear eddy-viscosity model sensitized to stress and strain invariants. Ph.D. thesis, Thermodynamics and Fluid Mechanics Division, Department of Mechanical Engineering, University of Manchester, UMIST, Manchester, U.K.

Sumitani, Y. and Kasagi, N. 1995. Direct numerical simulation of turbulent transport with uniform wall injection and suction. *AIAA J.*, **33,** 1220–1228

Suzuki, N., Matsumoto, A., Nagano, Y. and Tagawa, M. 1993. Anisotropy of heat transport and its modeling in homogeneous turbulent flow. *Heat Transfer—Japan. Res.*, **22,** 325–339

Taulbee, D. B. 1992. An improved algebraic Reynolds stress model and corresponding nonlinear stress model. *Phys. Fluids A*, **4,** 2555–2561

Tavoularis, S. and Corrsin, S. 1981. Experiments in nearly homogeneous turbulent shear flow with a uniform mean temperature gradient. Part I. *J. Fluid Mech.*, **104,** 311–347

Tzuoo, K. L., Ferziger, J. H. and Kline, S. J. 1986. Zonal models of turbulence and their application to free shear flows. TF-27, Thermosciences Division, Department of Mechanical Engineering, Stanford University, Stanford, CA

Vogel, J. C. and Eaton, J. K. 1985. Combined heat transfer and fluid dynamic measurements downstream of a backward-facing step. *J. Heat Transfer*, **107,** 922–929

Yakhot, V., Orszag, S. A., Thangam, S., Gatski, T. B. and Speziale, C. G. 1992. Development of turbulence models for shear flows by a double expansion technique. *Phys. Fluids A*, **4,** 1510–1520

Yang, Z. and Shih, T. H. 1993a. New time-scale-based k-ε model for near-wall turbulence. *AIAA J.*, **31,** 1191–1198

Yang, Z. and Shih, T. H. 1993b. A Galilean and tensorial invariant k-ε model for near-wall turbulence. NASA TM 106263

Yoshizawa, A. 1993. Bridging between eddy-viscosity-type and second-order models using a two-scale DIA. *Proc. 9th Symposium on Turbulent Shear Flows*, 23.1.1–23.1.6

Yoshizawa, A. and Nisizima, S. 1993. A nonequilibrium representation of the turbulent viscosity based on a two-scale turbulence theory. *Phys. Fluids A*, **5,** 3302–3304